

Molecular Mechanics and NOE Investigations of the Solution Structures of Intermediates in the [Rh(chiral bisphosphine)]⁺-Catalyzed Hydrogenation of Prochiral Enamides

Janet S. Giovannetti, Christine M. Kelly, and Clark R. Landis*

Contribution from the Department of Chemistry, University of Wisconsin, Madison, Wisconsin 53705, and Department of Chemistry and Biochemistry, University of Colorado, Boulder, Colorado 80309

Received August 24, 1992

Abstract: In order to probe the structural features that give rise to the high enantioselectivity observed for the hydrogenation of methyl (*Z*)- α -acetamidocinnamate (MAC) as catalyzed by complexes containing the fragment [Rh(chiral bisphosphine)]⁺, we have utilized NOE spectroscopy combined with molecular mechanics computations. In addition to the olefinic substrate MAC, we have examined its isopropyl ester (PRAC) and the diolefins norbornadiene and cyclooctadiene. Results are presented for the chiral bisphosphines DIPAMP, CHIRAPHOS, and DIPH. We address the following questions. (1) How does the chirality of the chiral bisphosphine ligand give rise to enantiodifferentiating interactions when a prochiral enamide is bound to the catalyst? (2) Are the solution structures of the catalysts similar to the crystallographically determined solid-state structures? (3) Can molecular mechanics computations account for the diastereoselectivities observed for the binding of the pro-*R* vs pro-*S* faces of MAC to the catalyst and for the rates of reaction of these intermediates with dihydrogen? The primary analytical methods employed are the SHAPES force field (for molecular mechanics computations) and conformer population analysis (CPA, for multiconformational analysis of NOE data) that have been developed in our laboratory. The results of these investigations demonstrate that these highly selective catalysts exhibit significant conformational mobility and the structure cannot be considered a rigid, chiral template. Overall, the solution and solid-state structures are similar, although both molecular mechanics and NOE investigations suggest that multiple conformers may be accessed. The principal enantiodiscriminating interaction appears to occur between the plane of the enamide ester function and the proximal arene ring of the chiral bisphosphine. We conclude that molecular mechanics computations can account for the binding diastereoselectivities of the antipodal faces of MAC to the catalysts but not for the relative reactivities of these intermediates with dihydrogen. As a result of the high steric energies computed by molecular mechanics, we cast doubt on the purported intermediacy of a six-coordinate dihydride in the catalytic asymmetric hydrogenation of prochiral enamides.

I. Introduction

The development of highly selective asymmetric catalysts is a prominent example of the important achievements in organotransition-metal chemistry during the past three decades.¹ Most noteworthy are the highly enantioselective epoxidation,² dihydroxylation,³ alkene isomerization,⁴ and hydrogenation catalysts.⁵ The asymmetric hydrogenation of prochiral enamides as catalyzed by cationic rhodium complexes containing chiral bisphosphines is a particularly spectacular example because of the high selectivity

* Correspondence should be addressed to this author at the University of Wisconsin.

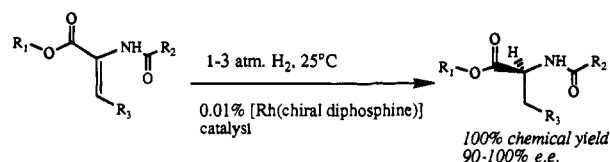
(1) (a) *Asymmetric Catalysis*; Bosnich, B., Ed.; NATO ASI Series; Martinus Nijhoff Publishers: Dordrecht, 1986. (b) *Asymmetric Synthesis*; Morrison, J. D., Ed.; Academic Press: New York, 1985; Vol. 5. (c) Noyori, R.; Kitamura, M. In *Modern Synthetic Methods 1989*; Scheffold, R., Ed.; Springer-Verlag: Berlin, 1989; p 115. (d) Brunner, H. *Top. Stereochem.* **1988**, *18*, 129. (e) Noyori, R.; Takaya, H. *Acc. Chem. Res.* **1990**, *23*, 345.

(2) (a) Zhang, W.; Loebach, J. L.; Wilson, S. R.; Jacobsen, E. N. *J. Am. Chem. Soc.* **1990**, *112*, 2801. (b) Jacobsen, E. N.; Zhang, W.; Muci, A. R.; Ecker, J. R.; Deng, L. *J. Am. Chem. Soc.* **1991**, *113*, 7063. (c) Katsuki, T.; Sharpless, K. B. *J. Am. Chem. Soc.* **1980**, *102*, 5974. (d) Gao, Y.; Hanson, R. M.; Klunder, J. M.; Ko, S. Y.; Masumune, H.; Sharpless, K. B. *J. Am. Chem. Soc.* **1987**, *109*, 5765.

(3) (a) Hentges, G. N.; Sharpless, K. B. *J. Am. Chem. Soc.* **1980**, *102*, 4264. (b) Jacobsen, E. N.; Marko, I.; Mungall, W. S.; Schroder, G.; Sharpless, K. B. *J. Am. Chem. Soc.* **1988**, *110*, 1968. (c) Wai, J. S. M.; Marko, I.; Svendsen, J. S.; Finn, M. G.; Jacobsen, E. N.; Sharpless, K. B. *J. Am. Chem. Soc.* **1989**, *111*, 1123.

(4) (a) Tani, K.; Yamagata, T.; Otsuka, S.; Akutagawa, S.; Kumoyashi, H.; Taketomi, T.; Takaya, H.; Miyashita, A.; Noyori, R. *J. Am. Chem. Soc.* **1982**, *104*, 600. (b) Inoue, S.; Takaya, H.; Tani, K.; Otsuka, S.; Sato, T.; Noyori, R. *J. Am. Chem. Soc.* **1990**, *112*, 4897. (c) Tani, K.; Yamagata, T.; Akutagawa, S.; Kumobayashi, H.; Taketomi, T.; Takaya, H.; Miyashita, A.; Noyori, R.; Otsuka, S. *J. Am. Chem. Soc.* **1984**, *106*, 5208.

of the transformation,⁶ the commercial value of the products,⁷ and the interesting mechanistic discoveries spawned by its development.⁸ With these "small molecule" catalysts, enzyme-



like enantioselectivity and catalytic activity (enantiomeric excesses >95% and limiting rates approaching 17 000 catalyst turnover/s) can be achieved in the hydrogenation of *N*-acetyldehydroamino

(5) (a) Horner, L.; Siegel, H.; Büthe, H. *Angew. Chem., Int. Ed. Engl.* **1968**, *7*, 942. (b) Knowles, W. S.; Sabacky, M. J. *J. Chem. Soc., Chem. Commun.* **1968**, 1445. (c) Knowles, W. S. *Acc. Chem. Res.* **1983**, *16*, 106. (d) Koenig, K. E. In *Asymmetric Synthesis*; Morrison, J. D., Ed.; Academic Press: New York, 1985; Vol. 5, Chapter 2. (e) Brown, J. *Angew. Chem., Int. Ed. Engl.* **1987**, *26*, 190. (f) Noyori, R. *Chem. Soc. Rev.* **1989**, *18*, 187.

(6) (a) Vineyard, B. D.; Knowles, W. S.; Sabacky, M. J.; Bachman, G. L.; Weinkauff, O. J. *J. Am. Chem. Soc.* **1977**, *99*, 5946. (b) Scott, J. W.; Valentine, D. *Science* **1974**, *184*, 943. (c) Knowles, W. S.; Sabacky, M. J.; Vineyard, B. D. *J. Chem. Soc., Chem. Commun.* **1972**, 10. (d) Fryzuk, M. B.; Bosnich, B. *J. Am. Chem. Soc.* **1977**, *99*, 6262. (e) Kagan, H. B.; Dang, T. P. *J. Am. Chem. Soc.* **1972**, *94*, 6429. (f) Achiwa, K. *J. Am. Chem. Soc.* **1976**, *98*, 8265.

(7) Knowles, W. S. *J. Chem. Educ.* **1986**, *63*, 222.

(8) (a) Halpern, J. *Science* **1982**, *217*, 401. (b) Brown, J. M.; Maddox, P. J. *J. Chem. Soc., Chem. Commun.* **1987**, 1276. (c) Chan, A. S. C.; Halpern, J. *J. Am. Chem. Soc.* **1980**, *102*, 5952. (d) Brown, J. M.; Chaloner, P. A. *J. Chem. Soc., Chem. Commun.* **1980**, 344. (e) Brown, J. M.; Chaloner, P. A.; Morris, G. A. *J. Chem. Soc., Chem. Commun.* **1983**, 664.

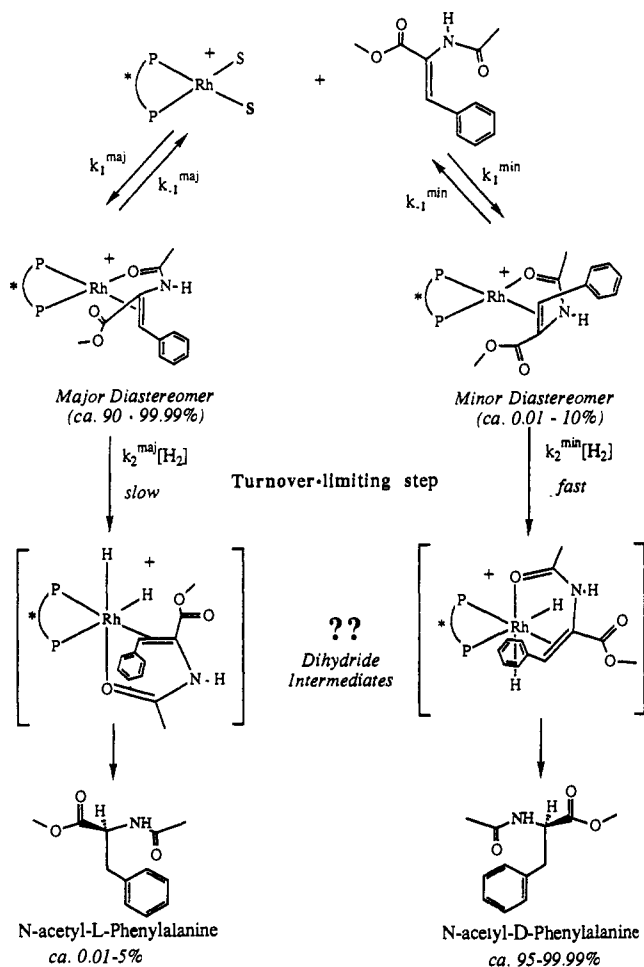


Figure 1. Mechanistic scheme for $[\text{Rh}(\text{chiral bisphosphine})]^+$ -catalyzed asymmetric hydrogenations of prochiral enamides. Question marks accompany the metal dihydroide complexes because these proposed intermediates have not been observed experimentally.

acid substrates, hereafter referred to as enamide substrates. The practical utility of this synthetic method has been demonstrated by the industrial production of L-DOPA via catalytic asymmetric hydrogenation.

The impact of the asymmetric hydrogenation reaction has not been limited to the synthetic arena, for it has proven to be a rich source of information concerning the mechanism of stereoselectivity control in metal-catalyzed reactions, also. These mechanistic studies have defined the sequence of kinetically relevant steps in the catalytic cycle (Figure 1). For the catalysts ligated by the DIPAMP bisphosphine, a quantitative evaluation of the corresponding rate constants and activation parameters has been reported by one of us.⁹ At common reaction pressures and temperatures, these kinetically relevant steps constitute diastereomeric manifolds comprising reversible binding of the enamide substrate to the metal followed by irreversible reaction with dihydrogen to produce the hydrogenated product. A notable feature of this mechanism, which appears to be general for a variety of different bisphosphine ligands, is that the more stable (2^{maj}) of the two diastereomeric catalyst-enamide adducts is virtually unreactive toward H_2 . In contrast, the less stable diastereomer (2^{min}) is so reactive toward H_2 that it more than compensates for a significantly lower (by 10-fold or more) equilibrium concentration of 2^{min} . Thus, the origin of selectivity lies not in the relative stabilities of the catalyst-enamide adducts but in their relative reactivities with H_2 .

Naturally, the high selectivities and unusual mechanistic features displayed by these catalysts raise a variety of questions.

(9) Landis, C. R.; Halpern, J. *J. Am. Chem. Soc.* **1987**, *109*, 1746.

What are the structures of the catalyst-substrate intermediates? Are the solution structures assumed by the catalysts similar to the crystallographic structures? Are the structures conformationally rigid or supple? What are the features that control the binding selectivity? Why does the reaction with H_2 favor the less stable diastereomer? In order to bring new light to these substantial but poorly understood issues, direct probes of the catalyst structure in solution are required. This paper describes our application of nuclear overhauser effect (NOE) methods, combined with molecular mechanics computations, to analyze the structures and energetics of intermediates in catalytic asymmetric hydrogenation.

It should be noted that these methods frequently are used in biophysical studies of, for example, the structures of biologically active peptides.¹⁰ In contrast, the application of these techniques to structural determination in transition-metal complexes is not well established;^{11,12} hence, a primary concern of this paper is the description of new methods that are appropriate for studying small transition-metal complexes.

Asymmetric hydrogenation catalysts are favorable test cases for these methods because (1) a large body of crystallographic, kinetic, and thermodynamic data has been accumulated for these compounds over the last two decades, (2) the reaction mechanism is well understood, (3) the catalyst substrate adducts are stable in solution for indefinite time periods, and (4) despite the synthesis of nearly 300 different catalysts designed for high selectivity, few of these exhibit selectivity patterns that are significantly different from the first bisphosphine-containing catalysts reported by Knowles,^{6c} Kagan,^{6e} Achiwa,^{6f} and Bosnich.^{6d} Noyori's RuBINAP catalysts^{5f} are recent notable exceptions. This last point suggests that very little is known about the critical structural attributes of these metal complexes that bestow such high selectivity on their catalytic transformations.

Our application of NOE and molecular mechanics methods focuses on a small set of asymmetric hydrogenation catalyst precursors and intermediates. The molecular mechanics computations examine a series of cationic rhodium complexes containing different chiral bisphosphine ligands: DIPAMP,^{6c,13} CHIRAPHOS,^{6d,13} and the ligand that we abbreviate as DIPH^{13,14} are shown in Figure 2. These complexes were chosen for investigation because the diastereoselectivities for binding the prochiral enamide MAC to these complexes are known. Quantitative NOE structural analyses of four complexes containing the DIPAMP ligand (**1a-4a**) are reported. Two of the complexes are intermediates in the asymmetric hydrogenation catalytic cycle: $[\text{Rh}(\text{DIPAMP})(\text{PRAC-d}_3)]^+$ (**4a**) (PRAC = isopropyl

(10) (a) Brooks, C. L.; Karplus, M.; Pettit, B. M. *Proteins: A theoretical perspective of dynamics, structure, and thermodynamics*. *Advances in Chemical Physics*; John Wiley and Sons: New York, 1988. (b) Brunger, A. T.; Kuriyan, J.; Karplus, M. *Science* **1987**, *235*, 458. (c) Kaptein, R.; Zuiderweg, E. R. P.; Scheek, R. M.; Boelens, R.; van Gunsteren, W. F. *J. Mol. Biol.* **1985**, *182*, 179. (d) Weiner, S. J.; Kollman, P. A.; Case, D. A.; Singh, U. C.; Ghio, C.; Alagona, G.; Profeta, S.; Weiner, P. *J. Am. Chem. Soc.* **1984**, *53*, 1. (e) Brooks, R.; Brucoleri, R. E.; Olafson, B. D.; States, D. J.; Swaminathan, S.; Karplus, M. *J. Comput. Chem.* **1983**, *4*, 187. (f) Wüthrich, K. *Acc. Chem. Res.* **1989**, *22*, 36.

(11) For examples of applications of molecular mechanics to transition-metal complexes, see: (a) Castonguay, L. A.; Rappé, A. K. *J. Am. Chem. Soc.* **1992**, *114*, 5832. (b) du Plooy, K. E.; Marais, C. F.; Carlton, L.; Hunter, R.; Boeyens, J. C. A.; Colville, N. J. *Inorg. Chem.* **1989**, *28*, 3855. (c) Brubaker, G. R.; Johnson, D. W. *Coord. Chem. Rev.* **1984**, *53*, 1. (d) Sironi, A. *Inorg. Chem.* **1992**, *31*, 2467. (e) Castonguay, L. A.; Rappé, A. K.; Casewit, C. J. *J. Am. Chem. Soc.* **1991**, *113*, 7177. (f) Hambley, T. W. *Inorg. Chim. Acta* **1987**, *137*, 15. (g) Lauher, J. W. *J. Am. Chem. Soc.* **1986**, *108*, 1521-1531. (h) Hancock, R. D. *Acc. Chem. Res.* **1990**, *23*, 253.

(12) For examples of the applications of NOE methods to transition-metal structure determination, see: (a) Alcock, N. W.; Brown, J. M.; Derome, A. E.; Lucy, A. R. *J. Chem. Soc., Chem. Commun.* **1985**, 575. (b) Walker, F. A.; Simonis, U. *J. Am. Chem. Soc.* **1991**, *113*, 8652. (c) Brunner, H.; Beier, P.; Riepl, G.; Bernal, I.; Reisner, G. M.; Benn, R.; Rufinakis, A. *Organometallics* **1985**, *4*, 1732.

(13) DIPAMP = (R,R)-1,2-bis[(o-methoxyphenyl)phenylphosphino]ethane; CHIRAPHOS = (2S,3S)-bis(diphenylphosphino)butane; DIPH = (R*,R*)-(±)-1,2-phenylenebis(methylphenylphosphine).

(14) Allen, D. G.; Wild, S. B.; Wood, D. L. *Organometallics* **1986**, *5*, 1009.

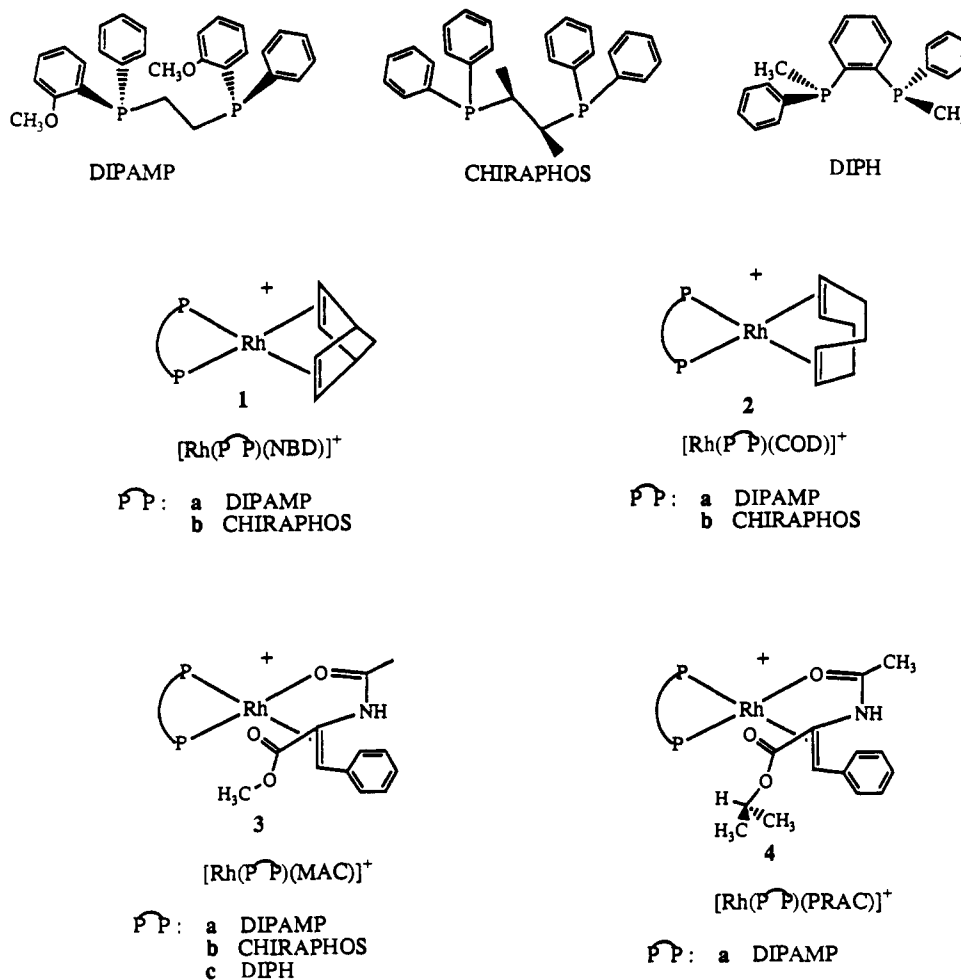


Figure 2. Structures and abbreviations of ligands and complexes examined in this work.

(*Z*)- α -acetamidocinnamate) and [Rh(DIPAMP)(MAC)]⁺ (**3a**). The other two complexes, [Rh(DIPAMP)(COD)]⁺ (**2a**) and [Rh(DIPAMP)(NBD)]⁺ (**1a**), are catalyst precursors for asymmetric hydrogenation. As the structures of these latter two complexes have been characterized in the solid state by X-ray crystallography, they are useful for comparing the results and techniques of solid-state and solution structural analyses.

Our initial approach in examining the origins of selectivity in asymmetric catalysis was to focus on stable, well-characterized *intermediates* in the catalytic transformation. Admittedly this approach does not directly address the control of product selectivity, which would require modeling of the reaction *transition state*. At the current level of force field development, a more elaborate analysis is unwarranted: even for far more thoroughly studied organic reactions, the modeling of transition states by molecular mechanics is controversial and difficult to evaluate. Therefore, in this paper we focus on evaluating the nature of solution structures and the stereodifferentiating interactions at selected stationary points along the catalytic cycle. As a crude probe of possible transition-state models for the turnover-limiting dihydrogen activation step, we examine the energetics of six-coordinate dihydride complexes.

II. Methods

A. NOE Data Collection and Analysis Techniques. Since the 1960s,¹⁵ the nuclear Overhauser effect has been used to characterize structural features of organic molecules in solution. Currently, NOE methods are used routinely for quantitative

mapping of three-dimensional structures, primarily for large biological molecules.¹⁶ The application of these methods to small molecules (MW < 1000) such as organotransition-metal complexes has been rare due to unfavorably short rotational correlation times and the resultant small NOE enhancements.

The determination of solution structures via NMR techniques comprises three parts:¹⁷ (1) assignment of all the proton resonances in the system, (2) collection of distance-dependent information using NOE experiments, and (3) structural refinement by fitting molecular parameters to best account for the NOE information. In the following sections we highlight the procedures used for the structural characterization of complexes built from the fragment [Rh(DIPAMP)]⁺; further details can be found in the Experimental Section and the cited references.

1. Assignment of Proton Resonances. Proton resonances for each complex were assigned using chemical shift,¹⁸ ¹H-¹H COSY,¹⁸ and ¹H-¹H TOCSY¹⁹ experiments. Assignments for [Rh(DIPAMP)(PRAC-*d*₅)]⁺ are given in Table I; tables of data for complexes **1a**, **2a**, and **3a** are available as supplementary material. Whereas the COSY experiment reveals a scalar coupling topology via cross peaks for coupled pairs, the TOCSY experiments give cross peaks throughout entire sets of sequentially coupled spins. This information is particularly useful for the assignments of overlapping arene resonances, since each arene ring comprises a sequentially coupled set. Previously, the elegant work of Brown and co-workers^{12a} demonstrated that COSY and steady-state

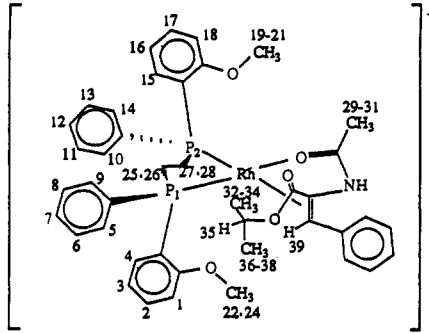
(16) Wüthrich, K. *Acc. Chem. Res.* **1989**, *22*, 36 and references therein.

(17) Williamson, M. P.; Neuhaus, D. *The Nuclear Overhauser Effect in Structural and Conformational Analysis*; VCH: New York, 1989.

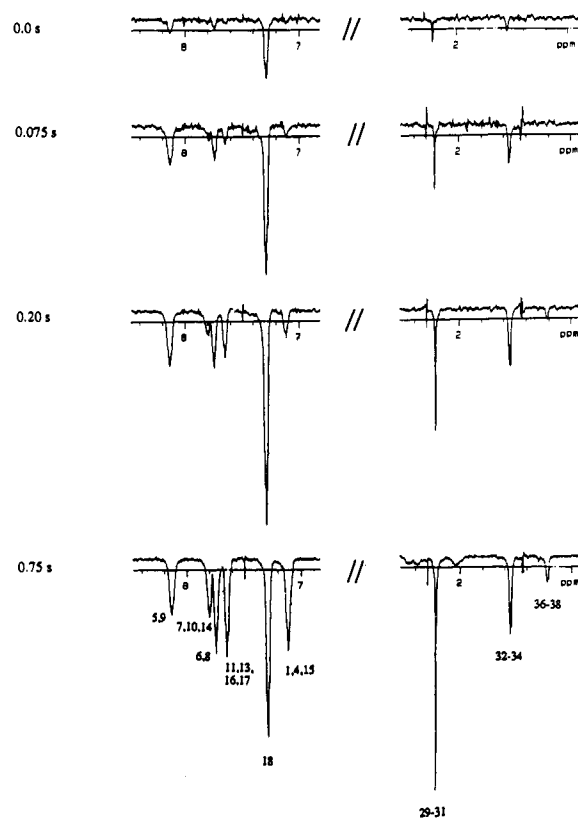
(18) Rance, M.; Sorensen, O. W.; Bodenhausen, G.; Wagner, G.; Ernst, R. R.; Wüthrich, K. *Biochem. Biophys. Res. Commun.* **1983**, *117*, 479.

(19) Bax, A.; Davis, D. G. *J. Magn. Reson.* **1985**, *63*, 355.

(15) (a) Anet, F. A. L.; Bourn, A. J. R. *J. Am. Chem. Soc.* **1965**, *87*, 5250. (b) Kaiser, R. *J. Chem. Phys.* **1965**, *42*, 1838. (c) Bell, R. A.; Saunders, J. K. *Can. J. Chem.* **1970**, *48*, 1114.

Table I. Resonance Assignments and Normalized Magnetization Intensities for Transient NOE Spectra of $[\text{Rh}(\text{DIPAMP})(\text{PRAC})]^+$ (**4a**) at Mixing Times of 0, 75, 200, and 700 ms


protons	chemical shift	inversion site protons					
		36-38	32-34	29-31	22-24	19-21	5, 9
36-38	1.22		2.966			3.000	3.000
			2.884			2.999	2.976
			2.785			2.985	2.961
			2.758			2.954	2.929
32-34	1.55	2.942				2.983	2.993
		2.806				2.937	2.950
		2.707				2.905	2.911
		2.738				2.866	2.896
29-31	2.20	3.000	2.992			2.983	
		2.990	2.985			2.961	
		2.986	2.980			2.916	
		2.972	2.955			2.841	
25-28	2.40 (br m)						3.000
22-24	3.00						2.998
							2.974
							2.928
19-21	4.15	3.000	2.986	2.986		2.986	2.986
		2.991	2.923	2.958		2.863	2.863
		2.971	2.864	2.913		2.773	2.773
		2.929	2.823	2.836		2.769	2.769
39	4.95			1.000	0.992	1.000	0.998
				0.956	0.964	0.980	0.926
				0.960	0.917	0.976	0.935
				0.954	0.875	0.962	0.914
35	4.99	0.950	0.949		1.000		0.985
		0.820	0.817		0.984		0.918
		0.698	0.703		0.990		0.901
		0.795	0.781		0.985		0.903
1, 4, 15	7.10	2.973	3.000	3.000	2.854	3.000	2.954
		2.928	2.981	2.990	2.580	2.981	2.819
		2.867	2.951	2.968	2.407	2.944	2.717
		2.805	2.870	2.922	2.326	2.770	2.673
18	7.28			1.000	0.998	0.883	0.995
				0.995	0.990	0.686	0.985
				0.983	0.991	0.561	0.970
				0.966	0.978	0.647	0.946
12	7.62						
11, 13, 16, 17	7.65			4.000	3.990	4.000	3.974
				3.998	3.956	3.9865	3.986
				3.980	3.916	3.904	3.956
				3.928	3.828	3.791	3.911
2, 3	7.72					1.988	
						1.937	
						1.664	
6, 8	7.75	2.000	1.977	2.000		1.985	1.858
		1.968	1.904	1.993		1.930	1.633
		1.937	1.848	1.989		1.882	1.472
		1.840	1.792	1.956		1.796	1.579
7, 10, 14	7.80	3.000	3.000	3.000	2.980	3.000	2.943
		2.970	2.978	2.995	2.946	2.977	2.891
		2.977	2.949	2.979	2.895	2.944	2.780
		2.931	2.894	2.933	2.832	2.869	2.703
5, 9	8.13	2.000	2.000		2.000	1.970	
		1.984	1.950		1.987	1.883	
		1.951	1.909		1.979	1.839	
		1.923	1.882		1.946	1.838	

**Figure 3.** One-dimensional transient NOE spectra obtained at four mixing times (0.0, 0.075, 0.20, and 0.75 s) upon inversion of the anisyl methoxyl resonance (protons 19-21, see Table I) of **4a** in ethylene glycol- d_6 at 10 °C. Because the NOE enhancements are negative and the spectra are obtained in the difference mode, the peaks grow in the direction of negative intensity.

NOE methods permit the assignment of all the proton resonances of the closely related iridium complex $[\text{Ir}(\text{DIPAMP})(\text{MAC})]^+$. Their assignments were used as starting points in our work.

2. Acquisition of ^1H - ^1H NOE Data. The nuclear Overhauser effect is a relaxation phenomenon that is revealed as changes in intensity of a NMR resonance when spin populations of another resonance are perturbed. The time courses of NOE intensities are sensitive to interproton separations (r^{-6}) and, thus, provide structural information in solution. A common problem in the characterization of small molecule structures by NOE methods is the small magnitude of NOE enhancements arising from the short rotational correlation times of small molecules in common solvents. However, this problem can be circumvented by the use of viscous solvents such as ethylene glycol.¹⁷ For example, selective irradiation at various resonances of $[\text{Rh}(\text{DIPAMP})(\text{MAC})]^+$ leads to interligand (between enamide and bisphosphine ligand sites) equilibrium NOEs which are small and positive in the low-viscosity solvent CDCl_3 (maximum NOE $\approx 3\%$, $\eta = 0.596$ cp at 25 °C), not observable in the more viscous solvent 2-propanol- d_8 ($\eta = 2.86$ cp at 8.5 °C), and large and negative in the most viscous solvent used, ethylene glycol- d_6 (maximum NOE $\approx -40\%$, $\eta = 19.9$ cp at 15 °C). Thus, the use of ethylene glycol effects large, negative NOE enhancements typical of molecules in the slow tumbling regime. It should be pointed out that viscous solvents do result in significant line broadening due to shortening of T_2 . Therefore, solvent viscosity must be manipulated to balance increases in NOE intensities with undesirable line broadening.

Structural information is derived from the transient NOE intensities as a function of the mixing time (i.e., the time elapsed since the inversion pulse).¹⁷ An example of a one-dimensional transient NOE time course for **4a** is presented in Figure 3; a complete tabulation of the data is given in Table I (tables of data for **1a**, **2a**, and **3a** are available as supplementary material). This

set of spectra, corresponding to irradiation of the anisyl methoxy resonance of **4a**, demonstrates the rapid growth of negative NOE intensities for nearby protons, linear during the initial growth period but deviating from linearity at longer mixing times as spin diffusion occurs. Note that nonzero enhancements are observed at a mixing time of zero. In the simple transient NOE pulse sequence used in this work, these enhancements evolve during the selective inversion pulse (i.e., a typical pulse length is 50 ms). Also shown is the delayed buildup of NOE enhancements at sites remote from the irradiated protons. These signs gain intensity predominately through spin diffusion across the aromatic rings.

3. NOE Data Analysis. The most common procedure for obtaining structures from NOE data is to derive interproton distances from NOE intensities and then to build structures that are consistent with those distances. Recently we have developed an alternative method,²⁰ conformer population analysis (CPA), that is a multiconformational approach to extracting structures from NOE data. Procedural details are provided in the Experimental Section.

CPA is based on the following assumptions. (1) Force field minimizations combined with systematic or Monte Carlo conformational searching techniques are capable of generating ensembles of conformers that are likely to be populated in solution (but may not be capable of calculating relative energies with sufficient accuracy to predict actual Boltzmann populations). These ensembles are used as trial structures for fitting to the NOE data. (2) The NOE intensity at each point in time represents the population-weighted sum of NOE intensities for each conformer in solution. It is assumed that conformer interconversion is slow compared with relaxation (T_1). Fitting of the calculated NOE intensities to the observed intensities is accomplished by varying the individual conformer populations until the best fit is obtained. (3) The best representation of solution structures is given by the most parsimonious collection of statistically significant conformers and their populations. The use of multiple conformations will always result in a fit to the data that is at least as good as the fit for a single conformation. However, it may not be significant to use, for example, four conformations rather than one. The CPA method uses the F-test to gauge the significance of using multiple conformations.

Note well that CPA differs from the more common distance-constrained methods in that the fitting degrees of freedom are the populations of the individual conformers; hence, multiple conformations are accommodated readily. Another advantage of the CPA approach is that overlapping resonances are accommodated in a natural way: the computed intensities of the overlapping resonances are summed. A unique solution to the observed NOE data generally does not exist. Therefore, each structure is analyzed with a minimum of nine analyses, each of which is initialized from a different starting point by varying the clustering level and/or clustering distance. Further discussion on the general problem of fitting structures to observed NOE data and on the attributes of the CPA method may be found in the cited literature.²⁰ We have reported previously that the CPA method is capable of recovering accurate conformer structures and populations from simulated data.

B. Molecular Mechanics Calculations. Previously we have described the SHAPES force field and its application to square planar complexes of rhodium.²¹ For the ligands the standard CHARMM^{10e} potential energy formulation was used. Standard CHARMM parameters were augmented with parameters for phosphine ligands that were developed in our laboratories. Metal-centered bond angle terms were treated with the SHAPES algorithms. These algorithms feature a spherical internal coordinate system and periodic Fourier angle bending terms. The SHAPES/CHARMM force field combination has been dem-

onstrated to reproduce bond lengths and angles at four-coordinate rhodium complexes to within ca. 0.02 Å and 3°, respectively.

The use of the SHAPES/CHARMM force field has been extended to six-coordinate dihydride rhodium complexes. The details of parameter development and final parameter values are given in the Experimental Section.

In comparing molecular mechanics-derived structures and energies with experimental results, the sampling of conformational space by the computational method is a concern of equal importance to the quality of the force field itself. In this work we have used two different protocols to search the molecular conformational space (details are provided in the Experimental Section). For the four-coordinate structures we used a three-step sequence of coordinate randomization, torsion angle grid search, and coordinate randomization. For the more crowded six-coordinate complexes, each increment of the torsion angle grid search was preceded by a stretching of the P-C_{arene} bond length. Several other schemes were tried, but for these crowded complexes we found that these procedures constitute a workable compromise between completeness and efficiency.

A persistently troublesome issue in molecular mechanics computations concerns the role of electrostatic interactions in controlling conformational energetics. In this work we have investigated the role of electrostatic interactions by carrying out computations with electrostatic interactions excluded entirely and by carrying out computations with point charges determined by the QEq method of Rappè and Goddard²² with a constant in vacuo dielectric constant. Solvent was not included in the simulations. In general we find that the inclusion of electrostatic interactions does not significantly alter the minimized geometries but may affect the conformational energetics. Therefore, our presentation of computational results are those without charges included unless explicitly stated otherwise.

III. Structures of Diolefin Complexes [Rh(bisphosphine)-(diolefin)]⁺

Due to their stability and ease of crystallization, many crystallographic structures have been determined for diolefin complexes with chiral bisphosphine ligands. In fact, it was based on these crystal structures that Knowles and co-workers first proposed that the critical attribute of successful asymmetric hydrogenation catalysts is the formation of rigid, chiral "edge-face-edge-face" arrays of arene rings attached to the phosphorus atoms (see Figure 4).²³ Working from a larger database, Oliver and Riley²⁴ demonstrated that in the solid state an edge-face-edge-face array is not a well-conserved feature of complexes containing chiral diphosphines and that one complex may crystallize in several conformationally distinct forms. Most recently, Brown and Evans²⁵ have performed a comprehensive analysis of structural features of crystallographically characterized asymmetric hydrogenation catalysts. They determined that (1) C₂-symmetric bisphosphines that form five-membered chelate rings generally conform to an approximate edge-face-edge-face array of arene torsions and (2) the edge-oriented arenes consistently occupy a pseudoaxial site on the chelate ring and the face-oriented arenes occupy a pseudoequatorial site.

Our primary interest lies in understanding how the chirality of the phosphine is sensed by the substrate. The closest contacts between a prochiral substrate and the chiral bisphosphine ligand occur at the arene rings of the phosphine ligand. Therefore, our analysis focuses on measuring the chirality of the arene ring conformations as defined in Figure 4. The first metric, the ϕ and ψ torsion angles, quantifies the edge vs facial orientation of the

(22) Rappè, A. K.; Goddard, W. A. *J. Chem. Phys.* **1991**, *95*, 3358.

(23) Koenig, K. E.; Sabacky, M. J.; Bachman, G. L.; Christopfel, W. C.; Barnstorff, H. D.; Friedman, R. B.; Knowles, W. S.; Stultz, B. R.; Vineyard, B. D.; Weinkauff, D. *J. Am. Chem. Soc.* **1980**, *102*, 333, 16.

(24) Oliver, J. D.; Riley, D. P. *Organometallics* **1983**, *2*, 1032.

(25) Brown, J. M.; Evans, P. L. *Tetrahedron* **1988**, *44*, 4905.

(20) Landis, C.; Allured, V. S. *J. Am. Chem. Soc.* **1991**, *113*, 9493.

(21) Allured, V. S.; Kelly, C. M.; Landis, C. R. *J. Am. Chem. Soc.* **1991**, *113*, 1.

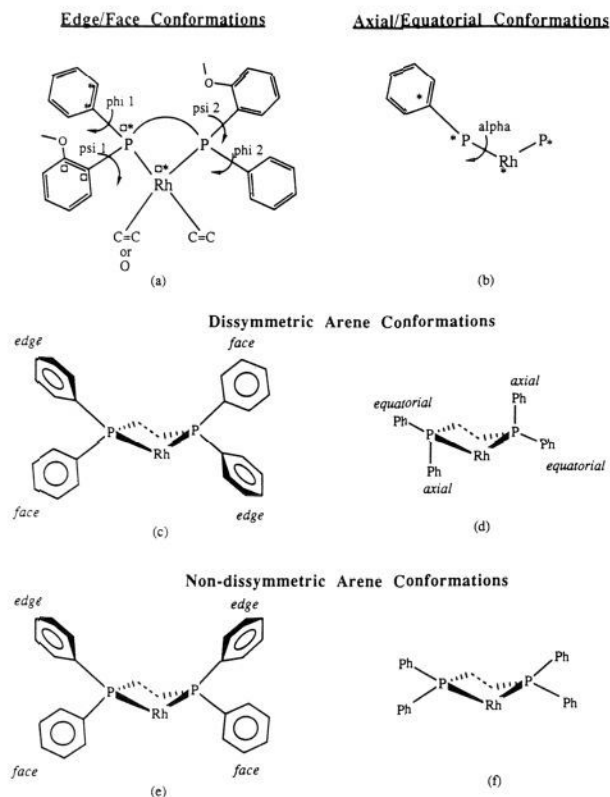


Figure 4. Torsion angle definitions and conformations of bis(diaryldiphosphino)ethane ligands coordinated to rhodium. (a) Definitions of ϕ (*) and ψ (□) torsion angles which describe the extent of edge facial orientation of the aryl rings: for the DIPAMP ligand the ψ label is always used for the anisyl aryl ring; angles labeled 1 are always coordinated trans to a C=C double bond. (b) The α angle defines the axial vs equatorial positioning of the aryl ring. Examples of chirality in the ϕ - ψ coordinates (c) and the α (d) coordinates are contrasted with nonchiral examples (e and f).

arene rings with respect to the P-Rh bond vector. These torsion angles have values of 90° and 0° for idealized edge and face orientations, respectively. The second metric, the α angles, quantifies the extent to which axial vs equatorial positions are assumed by the arene rings attached to each phosphorus. Idealized axial positions have values near 90° , and idealized equatorial positions have values near 135° for chelate rings in a half-chair conformation. In a very rough sense we may consider that chirality of the environment felt by the substrate is minimized when the arene ring orientations exhibit pseudo- C_2 symmetry in the arene orientations (here we are ignoring the conformation of the chelate backbone which is remote to the substrate). For example, edge-face-face-edge arrangements (Figure 4c) are less dissymmetric (or less chiral) than the strictly C_2 -symmetric arrangement, edge-face-edge-face (Figure 4e). The dissymmetry of the environment sensed by the substrate may be reduced in other ways; for example, by decreasing the puckering (Figure 4d) of the five-membered bisphosphine chelate ring so that pseudoaxial and pseudoequatorial positions are differentiated less (Figure 4f). In this section we present a detailed analysis of the conformations of the diolefin complexes $[\text{Rh}(\text{DIPAMP})(\text{COD})]^+$ and $\text{Rh}(\text{DIPAMP})(\text{NBD})^+$ as probed by force field computations, transient NOE experiments, and X-ray crystallography.

A. Computational and NOE Studies of $[\text{Rh}(\text{DIPAMP})(\text{COD})]^+$. Using grid search techniques that include full relaxation of all internal coordinates other than the two driven torsion angles, we have sampled the conformational energetics associated with rotation about the P-arene bonds. Shown in Figure 5 is the ϕ - ψ map for the COD complex $[\text{Rh}(\text{DIPAMP})(\text{COD})]^+$. Table II lists the values of important structural parameters, and Figure

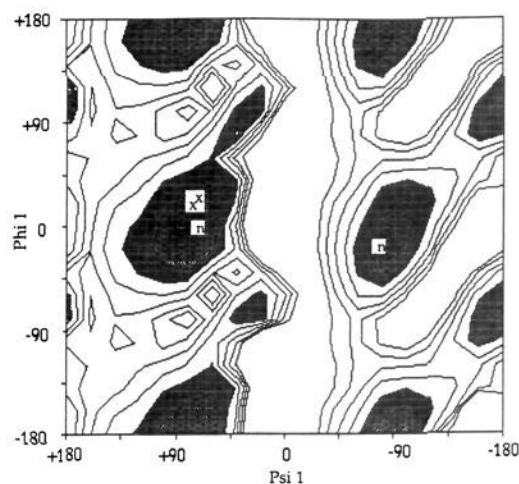


Figure 5. ϕ - ψ energy contour map for $[\text{Rh}(\text{DIPAMP})(\text{COD})]^+$ (1a). The ordinate of the plot corresponds to rotation about the P-C_{ipso} bond for the anisyl ring (ψ 1), and the abscissa describes rotation about the P-C_{ipso} bond for the phenyl ring (ϕ 1), as defined in Figure 4. Contours are drawn at 2 kcal/mol intervals. The lowest energy contour is darkest, and the adjacent contour, also, is darkened. The x markings indicate crystallographic values, and the n markings are for the best fit of the NOE data using three NOE time points and analysis by the conformer population analysis (CPA) method.

6 depicts the structures of pertinent complexes. Symmetry is a prominent feature of the map along the abscissa; rotation of an unsubstituted arene ring must generate redundant minima separated by 180° . Clearly the crystallographic structures lie in regions that are computed to be regions of minimum energy, thus lending confidence to the computational method and suggesting that crystal packing forces do not control the observed ϕ and ψ values.

The results of the conformer search computations generally are in agreement with the analyses of Brown and Evans.²⁵ The energy minima generally conform to an edge-face-edge-face array of ϕ - ψ - ϕ - ψ values, but the minima are quite broad. A sampling of α values in these regions reveals consistent puckering of the bisphosphine chelate ring. The arene rings assume well-differentiated pseudoaxial and pseudoequatorial positions (average α values of ca. 105° and 134° , respectively). These α values are loosely correlated with ϕ and ψ torsions: the axial rings tend to be edge and the equatorial rings facial. The regions of minimum energy are connected by low-energy (6–8 kcal/mol) distortion pathways, suggesting that arene ring rotation can occur readily in solution.

We have probed the influence of including atom-centered charges on the ϕ - ψ conformational maps (available as supplementary material). We find that the inclusion of charges does not change the disposition of the minima and, hence, the predicted structures but does increase the steepness of the contours. This result is in keeping with the conclusion of Smith and Karplus²⁶ that electrostatic interactions do not change dramatically the equilibrium geometries but do affect the relative energies of conformers.

Although the ϕ - ψ map contains regions of minimum energy around the crystallographic structure, this map suggests that other structurally inequivalent minima should be accessible. For the complexes containing the DIPAMP ligand, the methoxy groups of the facially directed ortho-anisyl ligand may be oriented toward the metal or away from the metal. For the COD complex, computations without electrostatics suggest that either conformation may occur; calculations with electrostatic terms favor the "in" orientation due to favorable interactions of the negatively charged methoxy group with the cation rhodium. The crystal

Table II. Structural Features of Crystallographic and Molecular Mechanics Structures for **1a**, **2a**, **3a-c**

[Rh(DIPAMP)(COD)] ⁺ (1a)													
	minimized structure		cryst		minimized structure		cryst		minimized structure		cryst		
Rh-P1	2.28	2.27	Rh-P2	2.28	Bond Lengths		2.26	Rh-D1	2.15	2.10	Rh-D2	2.16	2.15
P1-Rh-P2	80	83	P2-Rh-D1	173	Bond Angles		172	P2-Rh-D2	95	96	D1-Rh-D2	91	89
P1-Rh-D2	174	172	P1-Rh-D1	95	Torsions		96						
$\phi 1, \alpha$	-8, 106	10, 103	$\phi 1, \alpha$	77, 134	67, 137	$\phi 2, \alpha$	-4, 102	15, 99	$\phi 2, \alpha$	71, 137	64, 141		
[Rh(DIPAMP)(NBD)] ⁺ (2a)													
	minimized structure		cryst		minimized structure		cryst		minimized structure		cryst		
Rh-P1	2.23	2.27	Rh-P2	2.23	Bond Lengths		2.26	Rh-D1	2.10	2.10	Rh-D2	2.10	2.11
P1-Rh-P2	83	84	P2-Rh-D1	177	Bond Angles		173	P2-Rh-D2	100	102	D1-Rh-D2	75	70
P1-Rh-D2	175	170	P1-Rh-D1	102	Torsions		104						
$\phi 1, \alpha$	163, 115	174, 111	$\phi 1, \alpha$	-75, 128	-75, 122	$\phi 2, \alpha$	89, 147	113, 149	$\phi 2, \alpha$	-179, 96	170, 90		
[Rh(DIPAMP)(MAC)] ⁺ (3a)													
	minimized structure		cryst		minimized structure		cryst		minimized structure		cryst		
	major	minor	major	minor	major	minor	major	minor	major	minor	major	minor	
Rh-P1	2.25	2.26	2.27		Bond Lengths		2.12	Rh-D1	2.12	2.12	1.92		
Rh-P2	2.24	2.24	2.24				2.11	Rh-O	2.11	2.11	2.11		
P1-Rh-P2	83	83	83		Bond Angles		176	P1-Rh-D1	175	175	150		
P1-Rh-O	93	93	93				173	P2-Rh-O	174	174	173		
P2-Rh-D1	102	101	101		Torsions								
$\phi 1, \alpha$	69, 115	1, 128	48, 115		$\phi 2, \alpha$	-1, 97	109, 135	15, 107					
$\phi 1, \alpha$	22, 128	107, 114	52, 133		$\phi 2, \alpha$	60, 137	14, 99	61, 129					
[Rh(CHIRAPHOS)(MAC)] ⁺ (3b)													
	minimized structure		cryst		minimized structure		cryst		minimized structure		cryst		
	major	minor	major	minor	major	minor	major	minor	major	minor	major	minor	
Rh-P2	2.24	2.24	2.29		Bond Lengths		2.11	Rh-D1	2.12	2.12	2.07		
Rh-P3	2.24	2.24	2.23				2.11	Rh-O4	2.11	2.11	2.13		
P2-Rh-P3	83	84	83		Bond Angles		101	P3-Rh-D1	102	102	101		
P2-Rh-D1	175	174	163				175	P3-Rh-O	173	173	168		
P2-Rh-O	92	92	90		Torsions								
$\phi 1, \alpha$	87, 119	85, 133	22, 106		$\phi 2, \alpha$	14, 99	-28, 114	19, 101					
$\phi 1, \alpha$	-12, 125	9, 144	84, 133		$\phi 2, \alpha$	106, 136	98, 122	82, 135					
[Rh(DIPH)(MAC)] ⁺ (3c)													
	minimized structure		minimized structure		minimized structure		minimized structure		minimized structure		minimized structure		
	major	minor	major	minor	major	minor	major	minor	major	minor	major	minor	
Rh-P1	2.25	2.26	Rh-P2	2.23	Bond Lengths		2.23	Rh-D1	2.12	2.12	Rh-O	2.11	2.11
P1-Rh-P2	85	85	P1-Rh-O	92	Bond Angles		92	P2-Rh-D1	99	99	P2-Rh-O	169	165
P1-Rh-D1	175	176			Torsions								
$\phi 1$	110	172	$\phi 2$	-19	-36								

structure exhibits "in"-oriented anisyl rings. Thus, the computations suggest that conformations of the arene rings of the DIPAMP ligand that are not found in the crystallographic structure may be accessible. In principle, the further support for

the presence of the noncrystallographic conformations may be revealed by NOE measurements in solution.

Transient NOE spectra for the complex [Rh(DIPAMP)-(COD)]⁺ are dominated by strong *intraligand* cross-relaxations

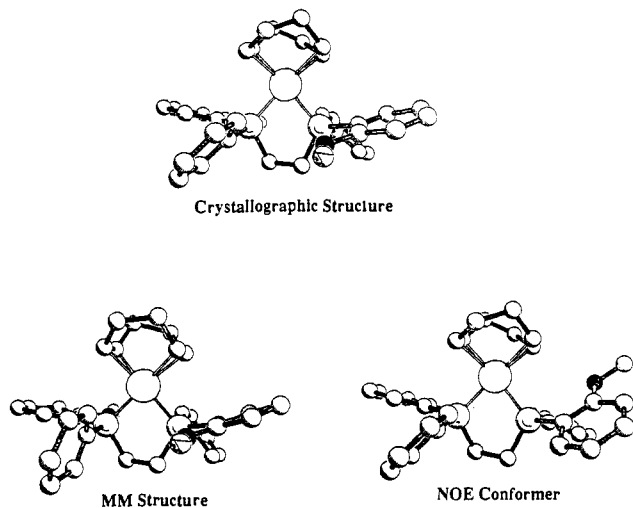
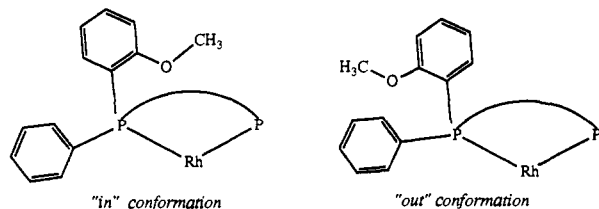


Figure 6. Crystallographic, molecular mechanics, and NOE (the predominant conformer only is shown) structures of $[\text{Rh}(\text{DIPAMP})(\text{COD})]^+$ (**1a**). All views are perpendicular to the coordination plane, and all hydrogens have been removed for clarity.



but clearly reveal *interligand* cross-relaxations as well. The primary *interligand* cross-relaxations involve the vinylic protons of the diolefin ligands and the arene rings of the bisphosphine. For this complex, a difficulty arises in the assignment of the vinyl protons. Two inequivalent sets of vinyl resonances are observed as expected for a diolefin coordinated to a C_2 -symmetric bisphosphine; therefore, two assignments patterns are possible. In principle, the NOE data can permit such a distinction. Refinements were performed with both sets of assignments, and the results were compared. One of the two assignments emerged as significantly superior (the *R*-factors approximately doubled, corresponding to a 0.001 significance level using the *F*-test method).

CPA analyses (Table III) of the NOE data for $[\text{Rh}(\text{DIPAMP})(\text{COD})]^+$ consistently refined to structures with edge-oriented phenyl rings and facially disposed anisyl rings. For example, a grouping of the initial set of 410 trial conformers into 20 clusters resulted in the population of two conformers (16% and 84% populations) with an *R*-factor of 0.39 on using a 0.05 significance level in the *F*-test phase. By increasing the clustering level to 50 or 75, the *R*-factor is lowered slightly to 0.38 and just one conformer is populated. The fitting solutions using clustering levels of 50 or 75 lead to the population of a conformer that is similar, although not identical, to those found using a clustering level of 20. At each clustering level, different groupings of structures obtained by changing the clustering distance measure (from r^{-6} to r^{-3} and r) did not change either the final conformers or populations.

It is interesting to note that, unlike crystallography, the appearance of C_2 symmetry in the NMR chemical shifts and coupling constants does not necessarily provide additional constraints in fitting of the NMR data of flexible conformers. The appearance of C_2 -symmetric resonance patterns in nonrigid systems may indicate either that the molecule populates conformers with static C_2 symmetry or that the molecule populates lower symmetry conformers in dynamic equilibrium with equally populated, C_2 -related images. For the latter case, the symmetry

Table III. Results of Conformer Population Analysis of Transient NOE Data for **1a**, **2a**, **3a**, and **4a**: Solutions with the Lowest *R*-factors Using Three and Four NOE Time Points

no. of time points	<i>R</i> -factor	rotational correlation time (ns)	conformer population	ϕ 1	ϕ 1	ϕ 2	ϕ 2
$[\text{Rh}(\text{DIPAMP})(\text{COD})]^+$ (1a)							
3	0.38	5.8	1.0	-35	-80	-4	75
4	0.44	6.6	0.88	-35	-80	-4	75
			0.12	-30	-100	-5	77
$[\text{Rh}(\text{DIPAMP})(\text{NBD})]^+$ (2a)							
3	0.36	1.8	0.43	100	-60	80	171
			0.39	100	-80	80	171
			0.18	160	-80	120	60
4	0.38	2.0	0.79	100	-80	80	171
			0.21	160	-80	120	60
$[\text{Rh}(\text{DIPAMP})(\text{MAC})]^+$ (3a)							
3	0.31	8.9	0.60	59	18	-3	120
			0.40	75	-14	-5	-60
4	0.38	7.9	0.66	59	18	-3	119
			0.34	100	-19	-7	0
			0.11	0	120	-8	66
3	0.28	7.0	0.40	90	-7	34	65
			0.38	89	4	74	45
			0.21	62	27	-6	-135
4	0.33	5.9	0.5	90	-7	34	65
			0.5	58	27	-6	-125

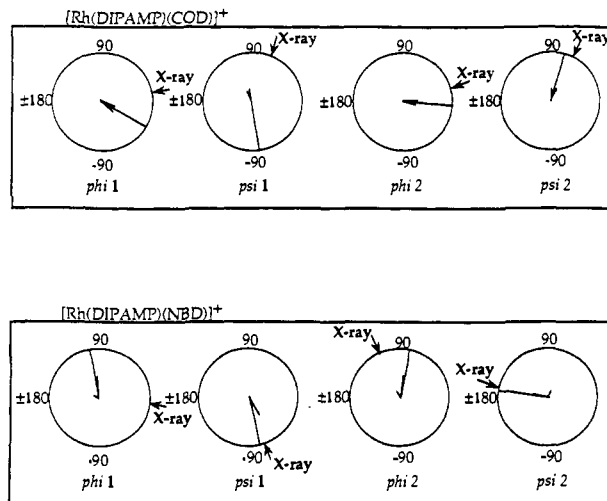


Figure 7. Dial diagrams for **1a** and **2a**. The lengths of the dials are proportional to the populations of the conformers accumulated over all analyses by the CPA method and the positions give the torsion angle values. Values from the crystallographic structures are indicated on the outer side of the dials.

does not lower the degrees of freedom in the fitting procedure. However, symmetry does reduce the amount of information contained within the NOE data as the total number of resonances and NOE cross peaks in the NMR spectrum is reduced.

A convenient method of presenting torsional data for multiple conformations is the "dial diagram" (Figure 7). An arrow on the exterior of the dial marks the torsional values for the crystal structure of each complex. On the interior of each dial is a set of vectors, each with length and direction corresponding to the populations and torsion angles, respectively, of the conformers obtained from CPA analysis. For the dial diagrams presented in this paper, the cumulative fractional populations for all analyses (with different clustering levels, numbers of time points, and clustering distances) are presented. Thus, the dials represent the summation of many different least-squares-fit solutions to the NOE data. For the DIPAMP complexes, phenyl ring torsion angles of θ and $\theta - 180$ are indistinguishable to the NOE experiment due to overlap of resonances on either side of the

arene rings. For these torsion angles, the diagram values were chosen to give the closer match with the crystallographic values.

The $[\text{Rh}(\text{DIPAMP})(\text{COD})]^+$ NOE data refine to unsymmetrical (non- C_2 -symmetric) structures (see Figure 7). Interestingly, both anisyl rings of the predominant conformer are facially oriented, but one anisyl ring adopts the "in" orientation and the other the "out" orientation. This is contrary to the crystal structure of the same complex but in agreement with molecular mechanics predictions. Examination of the cross-relaxation data reveals that this conformation represents a compromise to satisfying simultaneously strong NOE interactions between the vinyl resonances and both the anisyl methoxy and the anisyl protons that are *ortho* to the phosphorus. It should be noted that the data do not rule out other combinations of structures. For example, it is not possible to distinguish between the conformations obtained and a 50:50 mixture of conformers with both anisyl rings "in" and both rings "out", respectively.

The combination of crystallographic, molecular mechanics, and NOE-derived structural information for $[\text{Rh}(\text{DIPAMP})(\text{COD})]^+$ is brought together in the ϕ - ψ map (Figure 5) and molecular structure (Figure 6) depictions. With the exception of the "out"-oriented anisyl obtained from the NOE analysis, there is remarkably close agreement among the three methods. In fact, the "out" conformations suggested by NOE measurements do correspond to a region of low energy on the ϕ - ψ map. This suggests that the two conformations may be resolvable at lower temperatures.

Our CPA method relies on molecular mechanics for the generation of trial structures. However, the NOE analysis makes no use of the molecular mechanics energies in determining which of the available conformers should be populated. Therefore, the NOE structures are not constrained to regions of minimum energy on the ϕ - ψ map. We can consider the NOE structure and the ϕ - ψ map to be quasi-independent indicators of probable structures for $[\text{Rh}(\text{DIPAMP})(\text{COD})]^+$.

B. Crystallographic, Computational, and NOE Studies of $[\text{Rh}(\text{DIPAMP})(\text{NBD})]^+$. In order to increase the database of structural information for DIPAMP complexes we have determined the crystal structure of the complex $[\text{Rh}(\text{DIPAMP})(\text{NBD})](\text{PF}_6)$. The compound crystallizes with three crystallographically independent cations in each unit cell. However, only minor geometrical differences are observed among the three independent cations (Table II, Figure 8). The orientations of arene rings for the DIPAMP ligand in the solid-state configuration of the cation $[\text{Rh}(\text{DIPAMP})(\text{NBD})]^+$ do not adopt the edge-face-edge-face array found in the solid-state configuration of the cation $[\text{Rh}(\text{DIPAMP})(\text{COD})]^+$. The best description of the arene ring array (phenyl-anisyl-phenyl'-anisyl') for the crystallographic structure of the NBD complex is edge-face-face-edge. One of the anisyl rings has an edge disposition (ψ 2) and a strong axial placement. The arene rings of the other phosphorus exhibit less differentiation into axial and equatorial positions; the anisyl is arranged facially (and "out") with a slight equatorial disposition. With the omission of the methoxy groups of the anisyl and the backbone methylenes, this array can be considered to have pseudo- C_s symmetry (i.e., a mirror plane that bisects the P-Rh-P bond angle).

The small bite angle and rigidity of the NBD ligand strongly perturb the conformations available to this complex, as revealed by force field computations. Driving the ϕ and ψ torsion angles of the complex $[\text{Rh}(\text{DIPAMP})(\text{NBD})]^+$ with relaxation along all other degrees of freedom generates a severely "kinked" contour map (available as supplementary material). Strong van der Waals repulsions between the arene rings and the NBD ligand occur in the middle region of the map. Because of the driving procedure, the arene rings may be forced to overlap the nonbonding spheres of the vinylic carbons. The results are high steric energies and kinks in the contour maps.

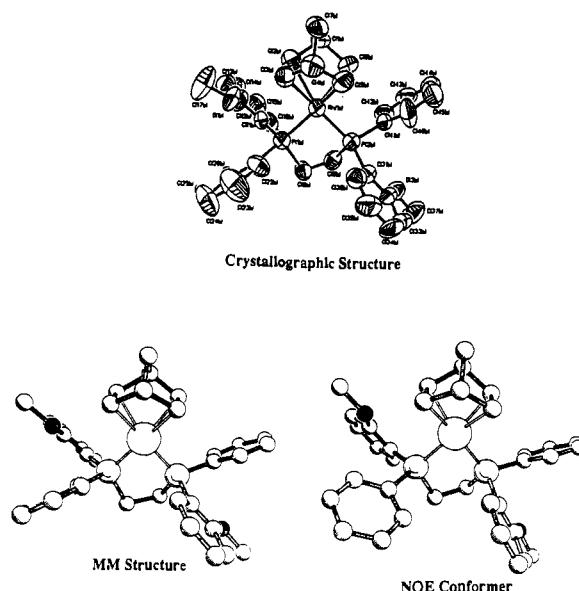


Figure 8. ORTEP plot of one configuration of the three independent crystallographic monocations found in the structural determination of the $(\text{PF}_6)^-$ salt of $[\text{Rh}(\text{DIPAMP})(\text{NBD})]^+$ (**2a**) shown with molecular mechanics and NOE-derived structures. All views are at ca. 75° with respect to the coordination plane, and all hydrogens have been removed for clarity.

The lowest energy structure of $[\text{Rh}(\text{DIPAMP})(\text{NBD})]^+$ is similar to the crystallographic structure in exhibiting an edge-face-face-edge array. As with the COD complex, low-energy pathways connect all regions of minimum energy, suggesting that the arene rings are free to undergo dynamic ring rotation (e.g., rotation of an anisyl ring from an "in" orientation to an "out" orientation).

As with the COD complex, the ^1H NMR spectrum of $[\text{Rh}(\text{DIPAMP})(\text{NBD})]^+$ exhibits a C_2 -symmetric pattern of resonances. Although the assignments of the vinyl resonances are not obvious, the NOE data are satisfied significantly better (at the 0.001 level of the F-test) with one of the two possible assignment patterns. Refinement of the NOE data (by use of three time points) by the CPA methods leads to the statistically significant population of three conformations (see Table III and Figure 7). The two conformers with highest populations differ in the ψ 1 value only. For these major conformers, one anisyl ring has an edge conformation, whereas the other anisyl ring adopts a facial "in" conformation. Here, the principal NOE interactions that are guiding the CPA analysis are the simultaneous presence of strong NOEs between the methoxy and vinyl (29, 32) protons and moderate NOEs between the same vinyl protons and *ortho* protons of the anisyl rings which lie on the ring edge that is opposite to the methoxy groups.

The conformer types that are populated by the CPA method are clustered near regions of minimum energy in the ϕ - ψ maps despite the exclusion of energetic information from the NOE analysis.

C. Discussion. Before turning to the enamide complexes of the $[\text{Rh}(\text{chiral bisphosphine})]^+$ fragment, we discuss some limitations and conclusions of the procedures discussed so far. Overall, we see encouraging agreement between molecular mechanics, crystallographic, and NOE-derived structures. Both molecular mechanics and NOE data analyses suggest that multiple conformations of the arene ring ϕ and ψ angles are possible; that is, the arene rings do not adopt a single chiral array. The very different arene ring orientations observed by crystallographic, molecular mechanics, and NOE computations for the NBD adducts of the $[\text{Rh}(\text{DIPAMP})]^+$ fragment, as compared with the COD adducts of the same fragment, illustrate well how the

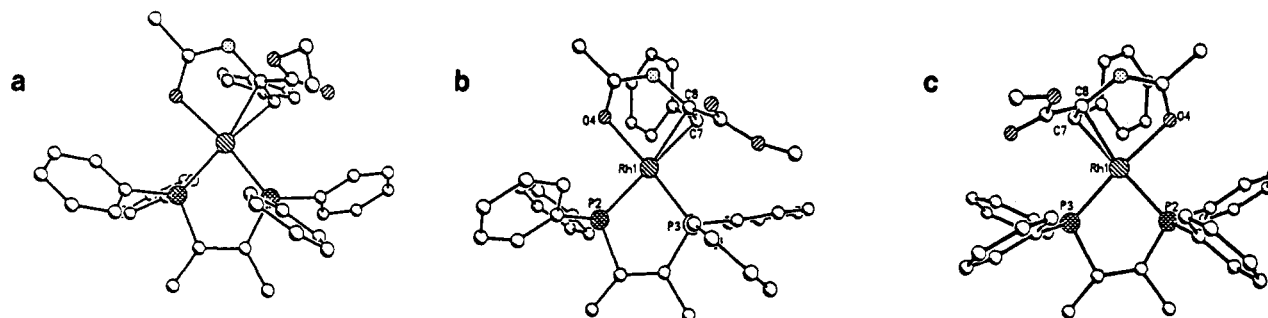


Figure 9. (a) Crystallographic structure of the major diastereomer of $[\text{Rh}(\text{CHIRAPHOS})(\text{EAC})]^+$ shown with the lowest energy molecular mechanics structure of (b) the major diastereomer of $[\text{Rh}(\text{CHIRAPHOS})(\text{MAC})]^+$ (**3b**) and (c) the minor diastereomer of $[\text{Rh}(\text{CHIRAPHOS})(\text{MAC})]^+$ (**3b**). All views are perpendicular to the coordination plane, and all hydrogens have been removed for clarity.

DIPAMP ligand flexes in response to the steric requirements of the diolefin substrates.

Perhaps the greatest source of concern in this analysis lies in the interpretation of the NOE data. Although NOE cross peak intensities are sensitive functions of interproton separations, the NOE studies suffer from uncertainties arising from (1) the possibility of systematic error in the data collection (due to incorrect resonance assignments, uncertainty in the rotational correlation times used, pulse imperfections, etc.), (2) the possibility of multiple fitting solutions, (3) the absence of the true structures in the basis set of trial structures, and (4) the influence of rapid conformer interchange.

Previously we have shown that conformer distributions are sensitive to the rotational correlation times.²⁰ We have not explored extensively the effect of changing the rotational correlation times in these studies. Optimization of the rotational correlation time using seven randomly selected structures from the trial set of conformers yielded similar results; the standard deviation of the isotropic rotational correlation times was less than 10% of the average value.

The uniqueness of the fitting solutions is difficult to evaluate. The results of the CPA analysis gave similar results (that is, conformers within one or two steps of one another on the grid search) regardless of the clustering distance measure employed and the number of clusters, indicating that the results are not strongly dependent on the starting point of the fitting problem. Nonetheless, it is possible that other solutions are equivalent to, or even better than, those found by the fitting procedure.

The CPA model used in this analysis assumes slow (with respect to T_1) conformer exchange. Because we anticipate, on the basis of the molecular mechanics torsion maps, rapid conformer exchange, the NOE fitting results will be affected. However, recent simulations of NOE spectra of these complexes in both the fast and slow conformer exchange limit do not show significant differences in the anticipated NOE enhancements.

It is appropriate to ask whether or not a multiconformational analysis is warranted. We cannot regard the choice of multiple conformations in the fitting procedure as indicating that multiple conformations must exist in solution, given the limitations of the fitting procedure and the data collection. However, we have shown that with the given relaxation model and with the structures available to the fitting procedure a *significantly* better fit is obtained with more than one conformer. The common set of NOE interactions that drives the CPA analyses to the use of multiple conformations appears to be the sizable NOE intensities between the vinylic hydrogens and protons located on both sides of the anisyl ring.

IV. Diastereomeric Complexes Containing Prochiral Enamides

Binding of the prochiral enamide to the $[\text{Rh}(\text{chiral bisphosphine})]^+$ fragment results in an equilibrium distribution of

diastereomeric adducts, corresponding to major and minor diastereomers in Figure 1. The equilibrium constant for these diastereomers varies with the nature of the chiral bisphosphine; for the enamide MAC, equilibrium constants of ca. >30, 10, and 1 are measured for complexes containing the chiral diphosphines CHIRAPHOS, DIPAMP,⁹ and DIPH,¹⁴ respectively. A primary purpose of our examination of these structures is to test whether the combination of molecular mechanics, NOE structural information, and crystallographic data can, with full appreciation of the limitations of these methods mentioned previously, provide both confidence in the application of these methods to homogeneous catalysis and insight into the nature of the stereodifferentiating interactions.

A. Molecular Mechanics Results. As with the diolefin complexes, the primary method of conformational searching for the enamide complexes was a three-step, fully relaxed grid search of arene torsions. Because the phosphorus atoms are inequivalent, two maps are shown per enamide isomer.

1. $[\text{Rh}(\text{CHIRAPHOS})(\text{MAC})]^+$. For the diastereomers of $[\text{Rh}(\text{CHIRAPHOS})(\text{MAC})]^+$, starting geometries were generated from the crystallographic coordinates for the related complex containing the ethyl ester of the enamide ligand $[\text{Rh}(\text{CHIRAPHOS})(\text{EAC})]^+$. The lowest energy structure for each diastereomer is shown in Figure 9, mean structural parameters are tabulated in Table II, and the ϕ - ψ maps for the two diastereomers are illustrated in Figure 10. The energies for the major and minor diastereomers are 70.2 and 72.5 kcal/mol, respectively, leading to a diastereomeric energy difference of 2.3 kcal/mol.

The ϕ - ψ maps of both diastereomers exhibit considerable flexibility in the orientation of the arene rings bonded to the phosphorus that is cis to the metal-coordinated amide carbonyl, as indicated by the broad low-energy contours. In contrast, the arene rings attached to the other phosphorus atom show narrower regions of minimum energy with the minor diastereomer accessing two nonredundant minima, whereas the major diastereomer accesses just one. The arene ring orientations found in the crystal structure^{9c} of the major diastereomer of $[\text{Rh}(\text{CHIRAPHOS})(\text{EAC})]^+$ are wholly contained within the lowest energy contour of the molecular mechanics map, indicating good agreement between solid-state structure and empirical computations.

2. $[\text{Rh}(\text{DIPH})(\text{MAC})]^+$. Although a crystallographic structure containing the $[\text{Rh}(\text{DIPH})(\text{MAC})]^+$ cation is not available, molecular mechanics structures may be generated readily. Selected mean structural parameters are shown in Table II. As the bisphosphine ligand contains just two arene rings, only one ϕ - ψ map is needed (available as supplementary material). A clear feature of these complexes is conformational flexibility: the ϕ - ψ map exhibits broad regions of minimum energy with low-energy barriers to ring flipping. Although the solution equilibria between major and minor diastereomers¹⁴ indicate very small energy differences (± 0.3 kcal/mol) that depend on the

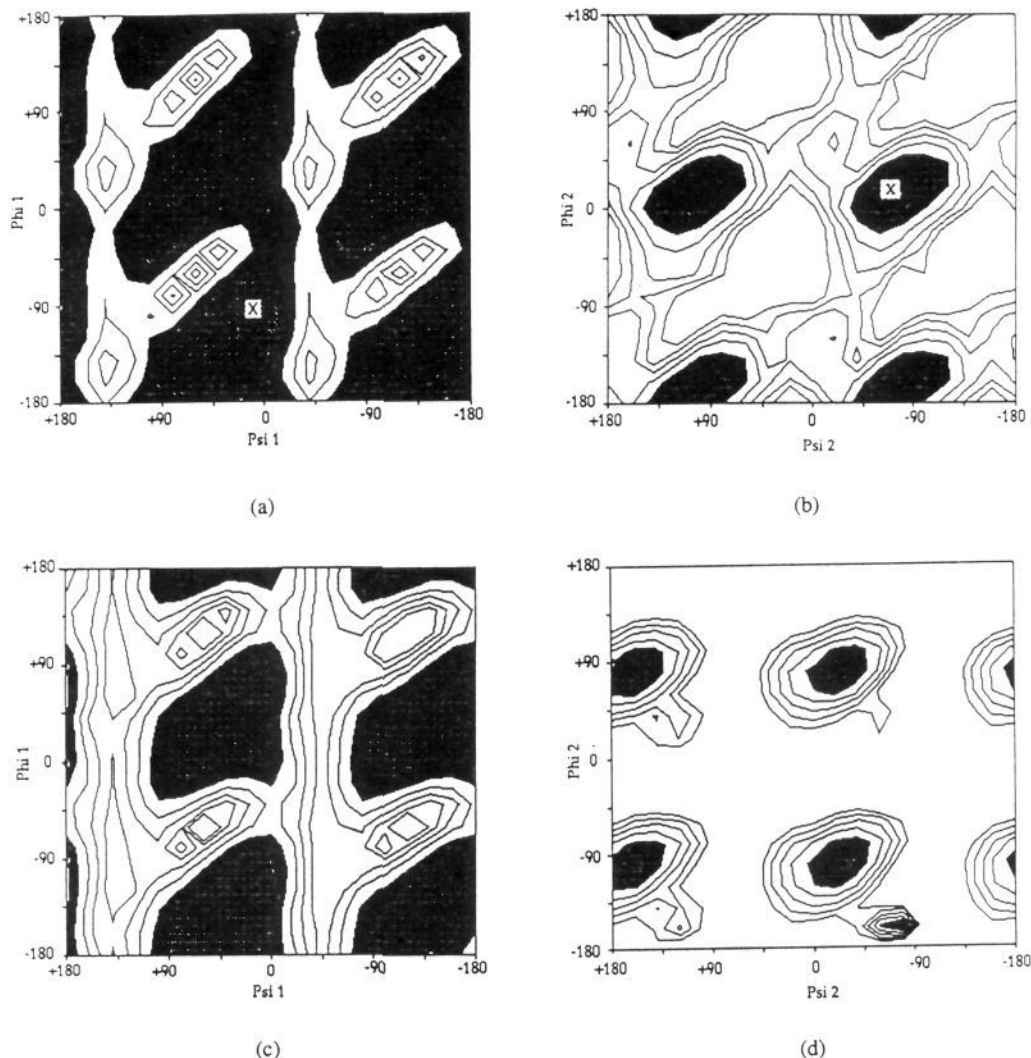


Figure 10. ϕ - ψ energy contour maps for the major (a and b) and minor (c and d) diastereomers of $[\text{Rh}(\text{CHIRAPHOS})(\text{MAC})]^+$ (**3b**). The angles labeled 1 are for the phosphorus that is coordinated trans to the enamide $\text{C}=\text{C}$ double bond, and the angles labeled 2 are cis. Contours are drawn at 2 kcal/mol intervals. The lowest energy contour is darkest, and the adjacent contour, also, is darkened. The x markings indicate crystallographic values of $[\text{Rh}(\text{CHIRAPHOS})(\text{EAC})]^+$.

Table IV. Molecular Mechanics Energies (kcal/mol) for $[\text{Rh}(\text{DIPAMP})(\text{MAC})]^+$ (**3a**) Diastereomers with λ and δ Chelate Backbone Conformations

	λ major	δ major	λ minor	δ minor
initial minimized energy	70.6	78.6	81.0	83.6
post-search lowest energy	69.6	72.4	73.8	70.0

solvent, our molecular mechanics computations suggest that the two diastereomers differ by 1.3 kcal/mol. The origin of these discrepancies is not clear, but the discrepancies do serve to illustrate that, at the current level of refinement, these force field algorithms and parameters cannot reliably discriminate energetic differences less than 1 kcal/mol.

3. $[\text{Rh}(\text{DIPAMP})(\text{MAC})]^+$. The DIPAMP-based catalysts are an interesting contrast to the CHIRAPHOS-based catalysts as these complexes have their centers of chirality located at the phosphorus atoms rather than on the chelate backbone. Only one complex of DIPAMP that contains a prochiral enamide has been characterized crystallographically,²⁷ the BF_4^- salt of $[\text{Rh}(\text{DIPAMP})(Z)\text{-}\beta\text{-propyl-}\alpha\text{-acetamidoacrylate}]^+$, which we will abbreviate as $[\text{Rh}(\text{DIPAMP})(\text{MPAA})]^+$. This complex differs

from the MAC complexes in that the enamide ligand is substituted with a propyl group at the β position of the $\text{C}=\text{C}$ double bond rather than with a phenyl group.

Five-membered chelate rings may adopt chiral, half-chair conformations, λ and δ , that differ in the orientation of the ligand backbone with respect to the plane defined by the metal and the two ligand coordination sites.²⁸ Because the ethane backbone spanning the two chiral phosphorus centers of the DIPAMP ligand is not substituted, there is no strong a priori preference for either the λ or the δ conformations. Using the three-step procedure described previously, we searched the conformational space of the four isomers (λ major, δ major, λ minor, and δ minor); energies of the lowest energy structures found for each search are presented in Table IV. Low-energy structures are shown in Figure 11, contour maps for the ϕ - ψ searches are shown in Figure 12, and mean structural parameters are tabulated in Table II. The following is observed. The lowest energy structure of the four diastereomers is the λ major stereoisomer, in keeping with the experimental observations of a λ conformation in the crystal structure for the BF_4^- salt of $[\text{Rh}(\text{DIPAMP})(\text{MPAA})]^+$ and greater stability for the major diastereomer (see Figure 11). For the major diastereomer, the alternative δ conformer is less stable than the λ conformer by 2.6 kcal/mol. As with the maps for the

(27) McCullough, B.; Halpern, J.; Thompson, M. R.; Landis, C. R. *Organometallics* **1990**, *9*, 1392.

(28) Corey, E. J.; Bailar, J. C. *J. Am. Chem. Soc.* **1959**, *81*, 2620.

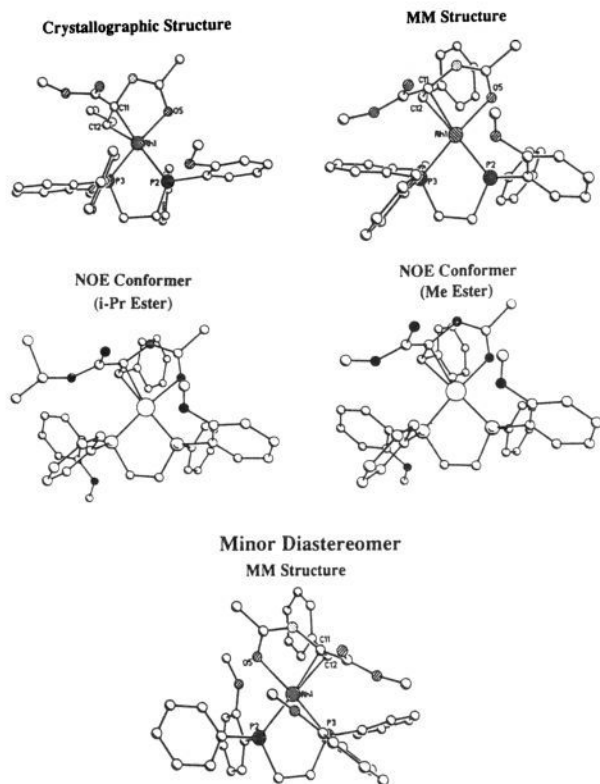


Figure 11. Crystallographic structure of the major diastereomer of $[\text{Rh}(\text{DIPAMP})(\text{MPAA})]^+$ shown with the lowest energy molecular mechanics structures of the major diastereomer of $[\text{Rh}(\text{DIPAMP})(\text{MAC})]^+$ (**3a**), the minor diastereomer of $[\text{Rh}(\text{DIPAMP})(\text{MAC})]^+$ (**3a**), and the NOE-derived structures (predominant conformer only) of the major diastereomers of **3a** and $[\text{Rh}(\text{DIPAMP})(\text{PRAC})]^+$ (**4a**). The views are perpendicular to the coordination plane, and all hydrogens have been removed for clarity.

$[\text{Rh}(\text{CHIRAPHOS})(\text{MAC})]^+$ complexes, the arenes rings bonded to the phosphorus located cis to the enamide ester group exhibit less conformational flexibility than the arene rings attached to the trans phosphorus.

An interesting result of the molecular mechanics investigations of the minor diastereomer is that the δ conformer is more stable: i.e., the reversal of the enantiotopic face of the enamide that is bound to the metal correlates with a change in ring conformation. The computed difference in energy between the lowest energy major and minor diastereomers of $[\text{Rh}(\text{DIPAMP})(\text{MAC})]^+$ is only 0.4 kcal/mol. This value is lower than the experimental ΔH of 1.4 kcal/mol. Experimental measurements indicate near zero entropies for the diastereomer equilibration. Although the correct diastereomer is found to be more stable, the estimated energetics (ignoring entropic considerations) are in error by about 1 kcal/mol.

Now we turn our focus to a fundamental question concerning selectivity in asymmetric hydrogenation of prochiral enamides: do molecular mechanics computations lead to simple models that explain stereodifferentiation in the binding of prochiral enamides? First we consider the rigidity of the edge-face-edge-face array of arene rings attached to the phosphorus atoms. *The shapes of ϕ - ψ maps and the positions of their minima for both the diolefin and the enamide complexes do not correspond exclusively to a single, chiral edge-face-edge-face array.* In particular, the complexes containing the strained diolefin norbornadiene exhibit substantial deviation from this idealized chiral array. In general, there appears to be some preference for a chiral edge-face-edge-face array of arene rings, but the arrangement is sufficiently supple to accommodate ligands which require other ring orientations.

Detailed consideration of the molecular mechanics maps for the CHIRAPHOS and DIPAMP complexes of the enamide MAC reveals surprisingly simple models for the origins of stereodifferentiation in substrate binding. For both complexes, a dominant steric interaction is that of the enamide ester group with the proximal arene ring of the bisphosphine ligand. In all of the complexes examined in this study, the planes defined by the enamide ester group and the nearby arene ring of the bisphosphine are approximately parallel. For the CHIRAPHOS ligand, changing from the major diastereomer is accompanied by a change from a half-chair five-membered ring conformation to an envelope conformation. The envelope conformation of the minor diastereomer minimizes steric contacts between the planes of the ester group and the proximal arene ring (Figure 13). However, this conformational change allows greater eclipsing of the backbone methyl groups with the phenyl groups of the phosphine, yielding a net destabilization of the minor diastereomer relative to the major diastereomer. This model emphasizes the requirement that the planes of the ester group and the proximal arene ring become as parallel as possible: i.e., an edge conformation of the proximal ring is preferred.

Similarly, the DIPAMP structures appear to be driven by minimization of steric interactions between the planes of the enamide ester group and the proximal arene ring of the phosphine ligand. Due to the lack of substituents on the chelate backbone, these complexes have a pathway available for avoiding these close contacts that does not disrupt the half-chair ring conformation: inversion of the chelate backbone from the λ to the δ conformation. This motion is accompanied by a small penalty, however. Inversion of the chelate ring allows the anisyl ring to adopt the axial-edge orientation favored by interactions with the substrate, but this places the bulkier anisyl ring, rather than the unsubstituted arene ring, in the pseudoaxial position. Axial placement of the bulkier arene is destabilizing due to 1,3-diaxial interactions. Thus, the diastereoselectivity of binding prochiral enamides to the $\text{Rh}(\text{DIPAMP})^+$ fragment can be attributed in part to the preference of the anisyl ring for the equatorial position. This model predicts that any substitution pattern that would cause the arene rings to have well-differentiated equatorial/axial positioning may be sufficient to induce significant asymmetry in the substrate binding environment. Knowles and others have demonstrated that analogues of the DIPAMP ligand in which the *o*-methoxy function of the anisyl ring is replaced by different functional groups (e.g., Cl, F) in either the ortho or meta position yield catalysts that exhibit high enantioselectivity in asymmetric hydrogenation.^{5c}

In summary, the molecular mechanics investigations, which do not include either solvent or entropic considerations, crudely account for the different stabilities of major and minor diastereomeric adducts of the $[\text{Rh}(\text{chiral bisphosphine})]^+$ fragment. However, the experimental free energy differences are small. Quantitative predictions of diastereomer stabilities at these modest levels of discrimination realistically cannot be expected or claimed. The value of these computations is that they lead to simple structural models of stereodifferentiation that ultimately can be tested and would be difficult to generate by any other method.

B. NOE Studies of $[\text{Rh}(\text{DIPAMP})(\text{MAC})]^+$ and $[\text{Rh}(\text{DIPAMP})(\text{PRAC})]^+$. Although crystallographic and molecular mechanics investigations yield similar structures for the major diastereomers of $[\text{Rh}(\text{DIPAMP})(\text{enamide})]^+$ complexes, there is little experimental information concerning the *solution structures* of either the major or the minor diastereomers. Brown^{12a} and Brunner^{12c} previously have reported qualitative steady-state NOE results for asymmetric hydrogenation catalysts. In particular the results of Brown are relevant to this work. On the basis of steady-state NOE data for the iridium complex $[\text{Ir}(\text{DIPAMP})(\text{MAC})]^+$ and the assumption of an edge-face-edge-face orientation of ligand arene rings, the absolute configuration of the major diastereomer of the iridium complex was proposed

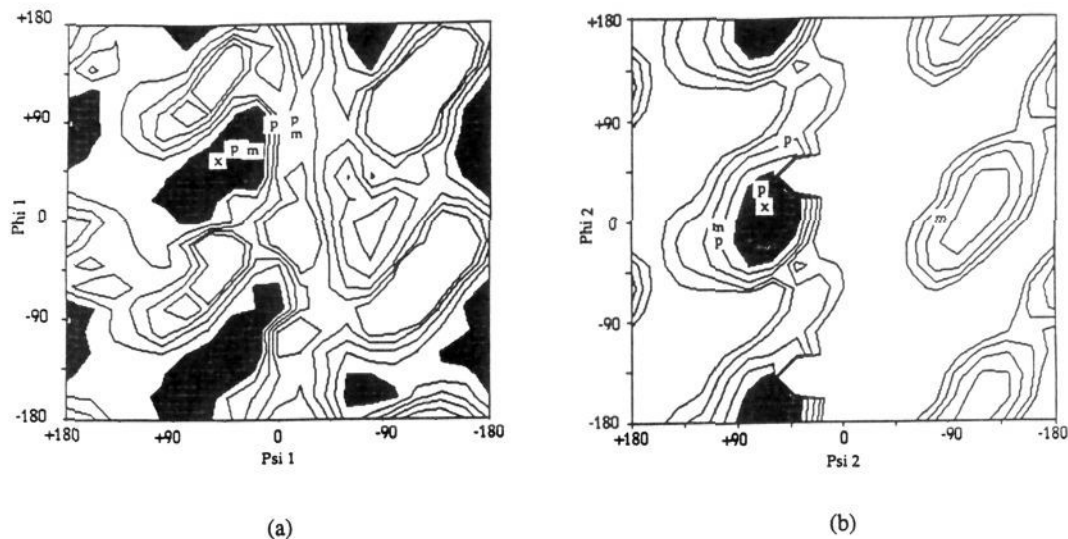


Figure 12. ϕ - ψ energy contour map for the major diastereomer of $[\text{Rh}(\text{DIPAMP})(\text{MAC})]^+$ (**3a**). (a) The angles labeled 1 are for the phosphorus that is coordinated trans to the enamide $\text{C}=\text{C}$ double bond, and (b) the angles labeled 2 are cis. Contours are drawn at 2 kcal/mol intervals. The lowest energy contour is darkest, and the adjacent contour, also, is darkened. The x markings indicate crystallographic values of $[\text{Rh}(\text{DIPAMP})(\text{MPAA})]^+$, whereas the p and m markings represent the positions for conformers giving the best fit to the NOE data for the PRAC- and MAC-containing complexes, respectively.

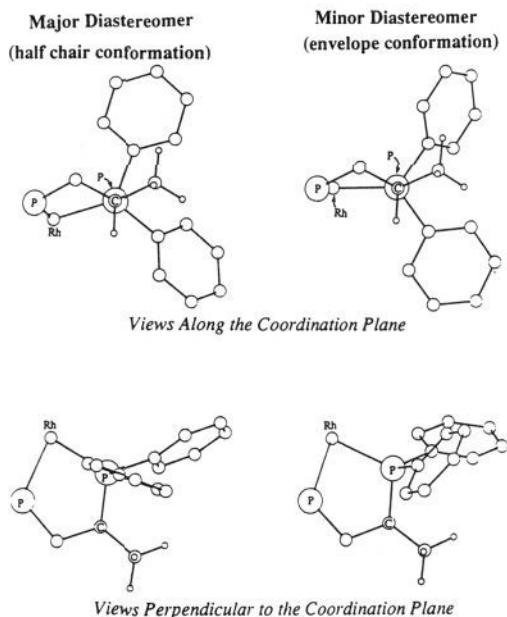


Figure 13. Conformations of the arene rings of major and minor diastereomers of $[\text{Rh}(\text{CHIRAPHOS})(\text{MAC})]^+$ (**3b**) computed by molecular mechanics. Newman projections looking down the $\text{C}_{\text{backbone}}-\text{P}$ bond for the phosphorus that is coordinated cis to the enamide $\text{C}=\text{C}$ bond exhibit a more staggered arrangement for the major diastereomer than for the minor diastereomer. The orthogonal views (from above the coordination plane) demonstrate the inversion of the face vs edge orientations of the arene rings for the major and minor diastereomers. For both diastereomers, the edge-oriented ring lies on the same side of the coordination plane as the enamide ester group.

to be the same as that for the rhodium analog. Due to the small NOEs observed in the low-viscosity solvent CDCl_3 , more detailed structural information could not be extracted for the iridium complex.

At the temperatures employed in the NOE studies (10°C), the concentration of the major diastereomer, which has coordination of the pro-R face of the $\text{C}=\text{C}$ double bond, is approximately 10-fold greater than that of the minor diastereomer. At this temperature, diastereomer interconversion is sufficiently slow compared with T_1 that the NOE data are not complicated by

chemical exchange. The diastereomer ratios measured in methanol and ethylene glycol are similar. Therefore, we conclude that the structural features controlling diastereoselectivity are not significantly different in the two solvents. An unfortunate difference between the two solvents, however, is that line broadening in ethylene glycol precludes direct observation of the proton resonances of the sparsely populated minor diastereomer. However, future studies using more finely tuned solvent viscosities and two-dimensional NOE techniques should allow us to probe the structure of the minor diastereomer as well.

Of all the complexes examined by NOE methods in this study, $[\text{Rh}(\text{DIPAMP})(\text{PRAC-}d_5)]^+$ has the most detailed NOE information and the most complete set of calibration points. The methyl groups of the isopropyl fragment are diastereotopic and clearly resolved in the ^1H NMR, leading to excellent calibration points. This inequivalence is revealed in the NOE data as well. For example, inversion of the methyl resonance (protons 36–38) exhibits a 3% interligand enhancement with the anisyl methoxy group (protons 19–21) at a 200-ms mixing time, whereas the enhancement is 13% for inversion of the diastereotopic methyl group containing protons 32–34. These data indicate unequal populations of rotamers generated by rotation about the oxygen-carbon bond of the isopropoxyl group.

All protons (the isopropyl, acetamido methyl, and vinyl groups) of the enamide ligand display strong NOE enhancements with at least one bisphosphine site at a 200-ms mixing time. Particularly strong NOE interactions that supply useful geometric constraints include that of the strong vinyl (proton 39) to both the anisyl methoxy (protons 22–24) and the *o*-phenyl (protons 5 and 9), the acetamido methyl (protons 29–31) to methoxy (protons 19–21), and the isopropyl methyl (protons 32–34) to methoxy (protons 19–21) cross-relaxations. Similar NOE behavior is seen for the complex of the enamide methyl ester $[\text{Rh}(\text{DIPAMP})(\text{MAC})]^+$.

The CPA analyses of the NOE data for $[\text{Rh}(\text{DIPAMP})(\text{PRAC-}d_5)]^+$ and $[\text{Rh}(\text{DIPAMP})(\text{MAC})]^+$ are shown in Table III. For both complexes the results are consistent; using a variety of different clustering levels (sorting the initial set of structures into 20, 30, and 40 clusters) and clustering distances (with r^{-6} , r^{-3} , and r -based distances) gives similar structures and populations (see the dial diagrams, Figure 14). Similar structures and populations are determined when just the first three mixing times

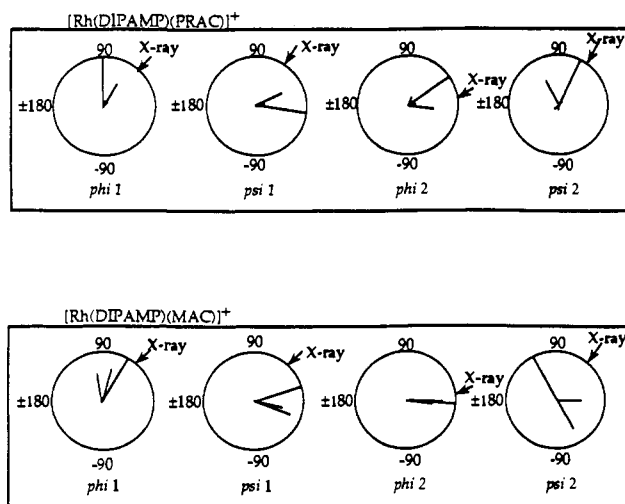


Figure 14. Dial diagrams for **3a** and **4a**. The lengths of the dials are proportional to the populations of the conformers accumulated over all analyses by the CPA method, and the positions give the torsion angle values. Values from the crystallographic structures are indicated on the outer side of the dials.

are used or when the fourth mixing time, for which spin diffusion effects are large, is included.

The structures that are populated in the CPA analysis of the major diastereomers of $[\text{Rh}(\text{DIPAMP})(\text{PRAC}-d_5)]^+$ and $[\text{Rh}(\text{DIPAMP})(\text{MAC})]^+$ exhibit considerable variation in arene ring orientation. Consider the two anisyl rings of the DIPAMP ligand. As in the low-energy molecular mechanics structures, the NOE analysis selects structures for which the phenyl ring that is proximal to the enamide ester group adopts an axial-edge orientation and the more remote anisyl ring adopts an equatorial-facial orientation. Once again we point out that the CPA method selects from the structures that are available without any bias from the structural energetics. For $[\text{Rh}(\text{DIPAMP})(\text{MAC})]^+$ the CPA method populates both "in" (approximately 65%) and "out" (approximately 35%) conformations of this anisyl ring; the "in" conformation only is populated for the isopropyl ester $[\text{Rh}(\text{DIPAMP})(d_5\text{-PRAC})]^+$. Fitting the $[\text{Rh}(\text{DIPAMP})(\text{MAC})]^+$ data by removing the "out" conformer results in a fit that is significantly worse as gauged by the F-test. Although statistically significant, it is not clear that this result is structurally significant. For the anisyl rings that are bonded to the phosphorus that lies trans to the $\text{C}=\text{C}$ of the enamide, the CPA analysis exhibits a slight preference for structures that have equatorial-edge-disposed anisyl rings and axial-facial phenyl rings. This preference is matched by the low-energy molecular mechanics structures.

C. Summary of NOE, Molecular Mechanics, and Crystallographic Results. The two principal methods used in this paper, NOE structure determination and molecular mechanics, are powerful yet are at an immature stage of development, especially for applications to organotransition-metal complexes. It should be recognized that, in contrast to the organic literature, a large body of experimental data to test these results against currently does not exist. Therefore, it is difficult to assess the accuracy of the structures and energetics of the methods employed. As a final point of validation, we ask if the available crystallographic, computational, and NOE-derived structures are consistent. In Figure 12, the positions of crystallographic and NOE structures are superimposed on a ϕ - ψ map for the major diastereomer of $[\text{Rh}(\text{DIPAMP})(\text{MAC})]^+$. Although the crystallographic structure is that of a different enamide, it is clear that both crystallographic and NOE experimental structures are clustered about minima in the molecular mechanics maps. A significant difference between the analysis of solution structures and crystallographic structures is conformational flexibility: the solution data may implicate more than just a single structure,

such as the "in" and "out" conformers of the anisyl rings of the DIPAMP-containing structures. It is satisfying that, although the solution structures arising from the NOE data for $[\text{Rh}(\text{DIPAMP})(\text{MAC})]^+$ are different from the crystallographic structures, these structures do lie near molecular mechanics minima. Taken together, molecular mechanics, NOE analyses of solution structures, and X-ray crystallography provide a remarkably self-consistent set of structures for these intermediates in asymmetric hydrogenation.

V. Addition of H_2 to Diastereomers of the $[\text{Rh}(\text{CHIRAPHOS})(\text{MAC})]^+$ and $[\text{Rh}(\text{DIPAMP})(\text{MAC})]^+$ Complexes

Examination of the stabilities of diastereomeric enamide complexes is useful for validation of these new methods but does not address the central issue of controlling the enantioselectivity of enamide hydrogenation. As mentioned in the Introduction, the enantioselectivity of prochiral enamide hydrogenation is not controlled by the relative stabilities of the diastereomers. Rather, it is the difference in the energies of the diastereomeric transition states for the addition of H_2 that is critical. We now turn our attention to simple models for mimicking the enantiodetermining H_2 addition transition states within the molecular mechanics force field framework.

In general, modeling of transition states for which changes in molecular topology occur (i.e., bonds are broken and made) is accomplished by developing molecular mechanics parameters for the transition state.²⁹ These methods may be criticized because many different parameters or transition-state models may lead to equally good correlations with experiment.³⁰ These models and parameters need not correspond to chemically reasonable values.

Transition-metal complexes present daunting obstacles to transition-state modeling: the computations are time-consuming, the results for simple stationary geometries may deviate significantly from experiment, and the experimental data available for comparison are limited. Brown and Evans²⁵ have used the transition state computed by Noel and Hay³¹ for addition of H_2 to $\text{Rh}(\text{PH}_3)_3\text{Cl}$ as a semirigid model for the addition of H_2 to the major and minor diastereomers of $[\text{Rh}(\text{CHIRAPHOS})(\text{MAC})]^+$. Brown and Evans as well as Bosnich and co-workers³² have attempted to model the entire progression of the reaction between H_2 and the four-coordinate diastereomers to yield the putative six-coordinate dihydride complexes $[\text{Rh}(\text{CHIRAPHOS})(\text{MAC})(\text{H})_2]^+$ using a rigid torsion driving procedure in which all bond angles and lengths were fixed and only the van der Waals energy terms contributed to the potential energy. As shown in Figure 15, a total of four isomers of $[\text{Rh}(\text{CHIRAPHOS})(\text{MAC})(\text{H})_2]^+$ arise from each diastereomer, depending on the trajectory of H_2 addition. Both Brown and Evans and Bosnich and co-workers concluded that addition of H_2 to the major and minor diastereomers was energetically viable for just one trajectory of H_2 addition per diastereomer. However, these studies are very crude; bond lengths and angles are held rigidly, the reaction paths are inflexible, only van der Waals potential energy terms are computed, the extent of conformational searching is unclear, and no systematic evaluations of the quality of the force fields for ground-state structures are presented.

We have used molecular mechanics to address two simple questions concerning the addition of H_2 to the diastereomers of $[\text{Rh}(\text{CHIRAPHOS})(\text{MAC})]^+$ and $[\text{Rh}(\text{DIPAMP})(\text{MAC})]^+$. Are there significant barriers in the accessibility of H_2 to the

(29) Houk, K. N.; Duh, H.; Wu, Y.; Moses, S. R. *J. Am. Chem. Soc.* **1986**, *108*, 2754.

(30) Menger, F. M.; Sherrod, M. J. *J. Am. Chem. Soc.* **1990**, *112*, 8071.

(31) Noell, J. O.; Hay, P. J. *J. Am. Chem. Soc.* **1982**, *104*, 4578.

(32) Bogdan, P. L.; Irwin, J. J.; Bosnich, B. *Organometallics* **1989**, *8*, 1450.

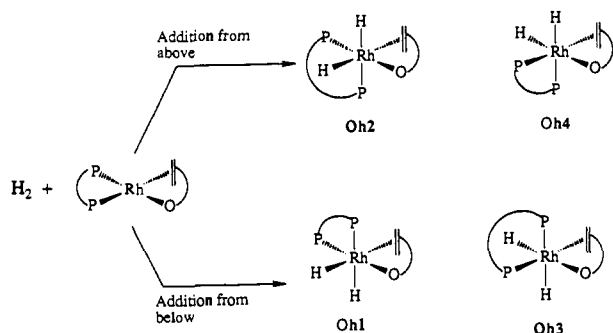


Figure 15. Schematic description of isomers that may be formed by cis addition of dihydrogen to square planar $[\text{Rh}(\text{bisphosphine})(\text{enamide})]^+$ complexes.

Table V. Low-Energy Dihydride Octahedral Isomers (kcal/mol)

	oh1 ^a	oh2	oh3	oh4
$[\text{RhH}_2(\text{CHIRAPHOS})(\text{MAC})]^+$				
major (70.178) ^b	114.0	112.6	110.1	104.8 ^c
minor (72.522)	<i>d</i>	<i>d</i>	103.8 ^c	104.0
$[\text{RhH}_2(\text{DIPAMP})(\text{MAC})]^+$				
major (69.623)	105.8	127.1	103.0 ^c	105.7
minor (70.020)	2115.1	106.1 ^c	113.3	125.6

^a Isomer notation illustrated in Figure 15. ^b Energy of the lowest four-coordinate square-planar structure. ^c Lowest energy isomer. ^d Structures were very skewed; correct isomeric relations were not maintained during minimization.

rhodium center? Are metal dihydride complexes appropriate models for the transition states of the H_2 addition reaction?

To enlighten our understanding of metal atom accessibility to incoming H_2 , we have taken the simple approach of slowly bringing the H_2 molecule toward the metal (using $\text{M}-\text{H}$ distance constraints) and computing the energies of the fully relaxed structures. For both diastereomers the H_2 was allowed to approach from above and below the coordination plane with both parallel and perpendicular orientations of the $\text{H}-\text{H}$ axis with respect to the coordination plane. This procedure can be revealing if and only if the steric energies incurred along the $\text{H}-\text{H}$ approach are such that a steric-dominated, early transition state is necessitated. We find no evidence requiring such an early transition state. All approaches permit the H_2 to arrive within 2 Å of the rhodium without substantial (>3 kcal/mol) energy penalties. For shorter $\text{Rh}-\text{H}$ separations, substantial orbital overlaps develop between the metal and H_2 ; simple molecular mechanics models are inappropriate.

A second approach to transition-state modeling focuses on the structures of the dihydride complexes of $[\text{Rh}(\text{CHIRAPHOS})(\text{MAC})(\text{H})_2]^+$ produced by oxidative addition of H_2 to the diastereomeric enamide complexes. If the oxidative addition pathway to yield, endergonically, a dihydride intermediate is indeed the pathway followed in the catalytic reaction cycle, then it follows from the Hammond postulate that the dihydride intermediate is an appropriate choice for a transition-state model.

Parameterization of the $\text{Rh}(\text{III})$ dihydride complexes is limited by the lack of available crystallographic structures. Therefore, our parameterization of octahedral complexes is based on analogy with four coordinate $\text{Rh}(\text{I})$ complexes; details are provided in the Experimental Section. The dihydride complexes $[\text{Rh}(\text{CHIRAPHOS})(\text{MAC})(\text{H})_2]^+$ and $[\text{Rh}(\text{DIPAMP})(\text{MAC})(\text{H})_2]^+$ are crowded, making conformational searching difficult. In order to sample the conformational space efficiently we have applied a "rubberband" search procedure (see Experimental) to each of the four dihydride structures per diastereomer. The energies of various dihydride isomers are shown in Table V.

Two remarkable features are revealed by these studies. First, there is a large increase (ca. 35–40 kcal/mol) in the total steric

energy in going from the four-coordinate structures to the six-coordinate dihydrides, reflecting the significant increase in unfavorable steric interactions. These increases principally are due to unfavorable steric interactions of the enamide ester group with the arene rings of the bisphosphine ligands. Second, the relative energies of the metal dihydrides derived from the major and minor diastereomers are not significantly different. Although the computations exhibit higher energies (by 1 kcal/mol) for the dihydrides derived from the major diastereomer than for the minor diastereomer of the CHIRAPHOS complex, the DIPAMP complex exhibits reversed relative energies. Furthermore, it appears that, in contrast with the findings of Brown and Evans²⁵ and of Bosnich and co-workers,³² the energies of many of the isomeric structures are sufficiently similar to make distinction between the likelihoods of various H_2 addition modes difficult. For example, addition of H_2 from either above or below the Rh coordination plane is plausible for all of the complexes.

All of the dihydride structures exhibit substantial deviation from idealized octahedral geometry. For example, in each structure the $\text{Rh}-\text{P}$ bond that is trans to a $\text{Rh}-\text{H}$ bond is significantly lengthened from its equilibrium value because of unfavorable interactions of the diarylphosphino group with the enamide ester. Other geometric parameters exhibit similar, large distortions from an idealized octahedral structure. The large increase in steric energies (ca. 40 kcal/mol) in going from the four-coordinate complexes to the six-coordinate dihydride complexes would not seem to be compatible with the very high hydrogenation rates that are observed experimentally (particularly since the formation of even sterically unencumbered dihydrides appears to be endergonic). Clearly the metal dihydride complexes generated by molecular mechanics are not good models for the transition state for the oxidative addition of dihydrogen. It is possible that the molecular mechanics parameters are too stiff; however, variation of parameters such as the angular distortion force constants does not change the results significantly. More likely, the transition state for the reaction bears little resemblance to a six-coordinate dihydride and, hence, a different computational model is required. We are in the process of performing detailed analyses of kinetic isotopic measurements to illuminate our understanding of the enantiodetermining H_2 activation reaction.

VI. Summary

We have presented detailed analyses of the structures and energetics of intermediates in asymmetric hydrogenation reactions using molecular mechanics, NOE, and X-ray crystallographic methods. Molecular mechanics results obtained with the parameters and algorithms of the previously described SHAPES force field are consistent with crystallographic structural parameters and quantitative measures of diastereoselectivity but should not be overextended. Structural characterization of asymmetric catalysts may be extended to liquid solutions by quantitative NOE studies aided by judicious manipulation of solvent viscosity. Multiconformational analysis of NOE data via the CPA method offers two major advantages: straightforward treatment of intensities involving unresolved resonances and the inclusion of multiple conformations when their use is judged to be statistically significant. The NOE-derived structures agree well with crystallographic structures and the locations of minima on conformational searching maps.

An important conclusion of these studies is that the chiral arene ring orientations are not rigid in these complexes. Substantial bisphosphine conformational changes occur as the substrate is varied. These changes include rotation of $\text{P}-\text{C}$ bonds (ϕ and ψ angles), distortion of the five-membered chelate rings from half-chair to envelope, and inversion of chelate ring chirality ($\lambda \leftrightarrow \delta$). Simple models for the origins of enamide diastereoselectivity focus on minimization of the steric interactions between the ester group of the enamide substrate and the proximal arene

ring of the phosphine ligand. The lower diastereoselectivity of enamide binding for DIPAMP vis-à-vis the CHIRAPHOS complexes is accounted for by the availability of the low-energy λ -to- δ chelate ring interconversion for the DIPAMP complex. Attempts to model the transition state of the hydrogenation reaction with six-coordinate metal dihydride complexes suggest that dihydrogen may add to either side of the four-coordinate square plane. However, these models fail to provide a quantitative accounting of diastereoselectivity in the H_2 addition step and suggest that dihydride complexes are too sterically encumbered to be viable intermediates in the hydrogenation reaction.

This work leaves many important questions unanswered, e.g., can NOE methods provide structural characterization of the less stable minor diastereomers, and what controls the selectivity of the dihydrogen addition reaction? Our future work is concerned with the refinement of the molecular mechanics and CPA computational techniques and their application to understanding existing highly selective catalysts and to designing new asymmetric catalysts.

VII. Experimental Section

A. Chemicals. Ethylene glycol- d_6 was freeze-pump-thaw degassed three times on a 1×10^{-7} Torr vacuum line and stored in an inert atmosphere glovebox.

B. Preparations. Isopropyl (*Z*)- α -acetamido- d_5 -cinnamate (PRAC- d_5), and methyl (*Z*)- α -acetamidocinnamate (MAC) were prepared by the method of Herbst and Shemin.³³ The diolefin complexes [Rh(DIPAMP)(NBD)](PF₆) and [Rh(DIPAMP)(COD)](BF₄) were prepared by standard methods. [Rh(DIPAMP)]₂(PF₆)₂ was prepared according to the method of Landis and Halpern.⁹ The [Rh(DIPAMP)-(enamide)](PF₆) complexes were prepared in an inert atmosphere glovebox by placing 7.0×10^{-5} mmol of [Rh(DIPAMP)]₂(PF₆)₂ and 2.1×10^{-4} mmol of enamide PRAC- d_5 or MAC, and ca. 0.7 mL of solvent in a 5-mm NMR tube, degassing with one freeze-pump-thaw cycle, and then sealing the tube.

All NMR sample concentrations were 0.02 M. Transient NOE experiments were performed with samples dissolved in ethylene glycol- d_6 .

C. Instrumentation. Proton NMR spectra were obtained at 500 MHz using a Varian VXR-500S spectrometer.

D. NMR Data Accumulation. 1. ¹H NMR Resonance Assignments. Assignments of the aromatic protons were made using chemical shift and scalar coupling information. The techniques used to obtain scalar coupling relationships between protons were ¹H-¹H double-quantum-filtered homonuclear correlation spectroscopy (dqf-COSY) and ¹H-¹H total correlation spectroscopy (TOCSY).

The following dqf-COSY pulse sequence of Rance et al.¹⁸ was used: $d_1, \pi/2, t_1, \pi/2, \Delta_1, \pi/2, aq$. Typically, 400 experiments of 16 scans each were performed, collecting 4096 points in F2. F1 and F2 spectral widths of ca. 800 Hz were used. The acquisition time for one scan was 2.546 s, and the Δ_1 mixing delay was 0 s. A short relaxation delay time (ca. 1.5 s) was used with a homospoil pulse during the delay. Quadrature detection in the second dimension was accomplished through the method of States and Haberkorn.³⁴ Zero filling to 1 K applying shifted sine bell weighting in both dimensions produced a absorption data matrix.

The following TOCSY pulse sequence of Bax et al.³⁵ was used: $d_1, \pi/2, t_1, \text{trim}, (\beta-\tau)_n, aq$. Typically, 400 experiments of 16 scans each were performed; 4096 points were collected in F2. F1 and F2 spectral widths of ca. 800 Hz were used. The acquisition time equaled 2.499 s, and delay and mix pulse times were relaxation delay = 1.5 s, trim = 3 ms, mix time = 70 ms. A $\pi/2$ pulse width for the normal transmitter power setting and a $\pi/2$ pulse width for the spin lock were calibrated by standard methods.³⁶ The transmitter power was adjusted to obtain a $\pi/2$ pulse of ca. 30 μ s for the spin lock pulses. Quadrature detection in the second dimension was accomplished through the method of States and Haberkorn.³⁴ Zero filling in F1 resulted in a 1K \times 1K matrix; shifted sine bell weighting was used in both dimensions.

(33) Herbst, R. M.; Shemin, D. *Org. Synth. Collect. Vol. II* 1943, 1.

(34) States, D. J.; Haberkorn, R. A.; Ruben, D. J. *J. Magn. Reson.* 1982, 48, 286.

(35) Bax, A.; Davis, D. G. *J. Magn. Reson.* 1985, 65, 355.

(36) Derome, A. E. *Modern NMR Techniques for Chemistry Research*; Pergamon Press: Oxford, 1987.

For the enamide complexes [Rh(DIPAMP)(PRAC- d_5)]⁺ and [Rh(DIPAMP)(MAC)]⁺, the presence of five inequivalent arene rings required the use of COSY, TOCSY, and NOE experiments for resonance assignments. The initial assignment required deuteration of the enamide arene ring ([Rh(DIPAMP)(PRAC- d_5)]⁺) in order to simplify the arene region of the spectrum. Resonance assignment began with the assignment of the single resonance at 8.15 ppm to the ortho protons (5 and 9) of the phenyl ring attached to the phosphorus cis to the double bond of the enamide. This assignment was suggested by the rather strong NOE enhancements at the enamide ester and vinyl resonances upon irradiation at 8.15 ppm. The ortho proton resonance exhibits a single cross peak in the COSY spectrum, thus identifying the resonance of the meta protons (6 and 8). Unfortunately, congestion close to the diagonal of the COSY spectrum does not permit unambiguous assignment of the para proton (7). However, the TOCSY spectrum displays two cross peaks along the trace at 8.15 ppm, one for the meta protons and one for the para proton. The latter cross peak fixes the chemical shift assignment for the para position. The anisyl ring protons labeled 1 and 18 are assigned readily due to a large NOE enhancement upon irradiation of the corresponding methoxy groups. The COSY and TOCSY spectra permit the remainder of the protons of the anisyl rings to be identified; however, spectral overlap prevents the assignment of a single proton to each unique resonance. Distinction between the two anisyl rings (i.e., which ring is located cis to the C=C bond of the enamide and which ring is located trans) is provided by the NOE data. Irradiation of the isopropyl methyl groups produces strong NOE enhancements with the anisyl ring (protons 1-4) attached to the P that lies cis to the C=C bond. Strong NOE enhancements are observed for the anisyl protons 15-18 upon irradiation of the acetamido methyl group (protons 19-21). The remaining arene ring was assigned by difference as it was the only unassigned spin coupling network in the TOCSY and COSY spectra.

Based on these initial assignments for [Rh(DIPAMP)(PRAC- d_5)]⁺, the identification of resonances in [Rh(DIPAMP)(MAC)]⁺ is straightforward. As with [Rh(DIPAMP)(PRAC- d_5)]⁺, the overlap of resonances resulting from the use of the viscous solvent, ethylene glycol, does not permit each proton to be correlated with a unique chemical shift. For the symmetrical (apparent C₂ symmetry from the equivalence patterns) complexes [Rh(DIPAMP)(NBD)]⁺ and [Rh(DIPAMP)(COD)]⁺ the COSY data combined with NOE information establish the assignment pattern with one ambiguity. The TOCSY, COSY, and qualitative NOE data do not provide data sufficient to identify which pair of vinyl resonances corresponds to which pair of inequivalent vinyl protons. This distinction can be made by quantitative NOE analysis only (see section IIIA).

2. T₁ Measurement. T₁'s were determined by the standard inversion recovery method.

3. Nuclear Overhauser Effect (NOE) Measurements. Equilibrium NOE's were measured using selective irradiation continued for a period of five times the T₁ value of the irradiated resonance. Two spectra were obtained, one spectrum with the perturbation to the system set on-resonance and one spectrum with the perturbation set off-resonance. Difference spectra were obtained by subtracting the Fourier-transformed off-resonance spectra from the Fourier-transformed on-resonance spectra, (I - I₀).

The following pulse sequence was used in the transient NOE experiments:³⁷ selective $\pi - \tau - \pi/2$. These data were acquired in the difference mode. Each spectrum used a spectral width of ca. 4000 Hz; 16 384 points were collected with an acquisition time of 1.895 s. Presaturation of the solvent hydroxyl resonance during the relaxation delay was performed for samples dissolved in ethylene glycol- d_6 . A relaxation delay of five times the longest T₁ (15-19 s) was used for each experiment to allow full longitudinal relaxation between pulses. Non-selective $\pi/2$ pulses and selective π pulses were calibrated by standard methods before each experiment. Exponential apodization with line broadening of 1 Hz was applied before each Fourier transform. A spline base line correction was applied to maximize the accuracy of measured integrals. Growth of NOEs was observed by collection of difference spectra with incremental τ values. The linear portion of the NOE growth curve for the complexes is measured to be 0-150 ms; the NOE growth curve reaches an inflection point after ca. 0.8 s. For each of the complexes [Rh(DIPAMP)(PRAC- d_5)](PF₆), [Rh(DIPAMP)(MAC)](PF₆), [Rh(DIPAMP)(NBD)](PF₆), and [Rh(DIPAMP)(COD)](BF₄), two data sets were acquired. One data set with τ values of 60 and 100 ms was obtained for analysis using the isolated spin pair approximation (not reported in this paper). Another data set with τ values of 0, 75, 200, and

(37) Gordon, S. L.; Wüthrich, K. *J. Am. Chem. Soc.* 1978, 100, 7094.

700 ms was acquired for analysis using the full relaxation matrix method. All intensity data are presented as normalized magnetization intensities with an intensity of 1.0 corresponding to the integrated area for a single proton. Measurements were made at 10 °C for [Rh(DIPAMP)(PRAC-*d*₅)](PF₆), [Rh(DIPAMP)(MAC)](PF₆), and [Rh(DIPAMP)(COD)](BF₄) in ethylene glycol-*d*₆. Measurements were made at -13 °C for [Rh(DIPAMP)(NBD)](PF₆) in a 3:2 mixture of ethylene glycol-*d*₆ and methanol-*d*₄. Low solubility of the complex in ethylene glycol-*d*₆ necessitated the use of a solvent mixture; the temperature was decreased to obtain a similar solvent viscosity.

E. NOE Data Analysis. 1. Generation of Trial Structures. Systematic dihedral driving using a modified version of the CHARMM^{10c} molecular mechanics program which includes the SHAPES force field²¹ was performed. Rh-P-C_{ipso}-C_{ortho} dihedral angles were systematically varied in 20° increments for phenyl and anisyl rings attached to P2 and varied in 60° increments for the phenyl and anisyl rings attached to P3 for [Rh(DIPAMP)(MAC)]⁺, [Rh(DIPAMP)(PRAC-*d*₅)]⁺, [Rh(DIPAMP)(COD)]⁺, and [Rh(DIPAMP)(NBD)]⁺. The geometric parameters were varied iteratively to a minimum energy using 250 (for structures generated at 60° intervals) or 500 (for all others) adopted basis Newton Raphson steps. The energy was evaluated after each variation in dihedral angles. All structures were saved, resulting in 361 structures from variation by 20° increments about P-C_{arene} and 49 structures from variation by 60° increments about P-C_{arene} for each complex. In addition to the systematic searches, an additional set of approximately 25 structures was generated using the Boltzman jump random torsion-space search algorithm contained with the QUANTA software package.³⁸

In this work all structures generated by the conformational searches were used in the data analysis. Therefore, the molecular mechanics energies have no influence on the structure refinement. A more efficient, although biased, conformer population analysis would be based only on structures with energies that are lower than some cutoff value.

2. Clustering. Clustering, used here as a data reduction technique,²⁰ is based on grouping a large set of structures into clusters such that structures within a cluster have maximum similarity. Various schemes for measuring the similarity of structures exist; this work utilizes the Euclidean distance metric. The Euclidean distance between two structures (*D*_{ab}) is computed from the differences between interproton separations for all proton pairs exhibiting cross-relaxations in the NOE spectrum.²⁰ Because we wish to cluster structures based on similarities as seen by the NOE experiment, the interproton separations raised to the -6 power are used for most analyses. Structures were clustered by a two-step process: an initial configuration was generated by the hierarchical method followed by application of the K-means clustering algorithm. In general, the optimal number of clusters to use in a particular analysis cannot be defined. Because clustering is used as a data reduction technique, we use a number of clusters (or clustering level) that is less than the number of NOE observations. Clustering levels of 20, 50, and 75 were used in each of the analyses; in effect, different starting points for the fitting procedure and generated by using different clustering levels. Another method of generating different starting points for the fitting procedure is to change the similarity metric, that is the Euclidean distance computation. At each clustering level, we generated clusters with Euclidean distances calculated using interproton separations raised to the 1, -3, and -6 powers.

3. Computation of NOE Intensities. A full relaxation matrix analysis (FRMA) was used. For each structure an NOE time course is computed by numerical integration of the coupled Solomon equations³⁹ (eq 1),

$$\frac{\partial I_j}{\partial t} = -\sum_{n \neq j} (\omega_{0jn} + 2\omega_{1jn} + \omega_{2jn})(I_j - I_{0j}) - \sum_{n \neq j} (\omega_{2jn} - \omega_{0jn})(I_n - I_{0n}) \quad (1)$$

where the transition probabilities, ω_{xjn} , depend on the interproton separations and the correlation times *t*. Numerical integration was performed using the variable step Runge-Kutta algorithm. Because methyl groups may have internal motions whose rates are competitive with molecular rotations, a simple three correlation time model (τ values) is used. The three correlation times used correspond to effective correlation times for methyl-methyl, methyl-nonmethyl, and nonmethyl-nonmethyl dipolar couplings. Calibration of the effective correlation times was made by simplex optimization using NOE data for protons with fixed interproton

separations. The magnetization of each proton is computed as a function of time and the individual magnetizations of equivalent or overlapping resonances are summed to give the group resonance intensities.

4. Least-Squares Fitting. Least-squares fitting of the NOE data was performed using a constrained least-squares analysis. For these analyses the conformers are assumed to interconvert slowly. According to this approximation, the net NOE intensities *I_j(t)* are represented by the population-weighted sum of NOE intensities (eq 2). In the clustering

$$I_j(t) = \sum_a \rho_a I_{j_a}(t) \quad (2)$$

phase of the analysis, the conformers used in the fitting were the structures that were closest to each of the cluster centroids from the preceding data reduction cycle. In the F-test phase of the analysis, the structures used in the fitting were obtained by deletion of the least populated conformer from the previous fit. The conformer populations are constrained such that negative populations are not allowed and the total sum of the fractional populations is 1.

5. Solution Structure Refinement. Refinement of the conformer populations was accomplished by expanding the basis set of conformers to include all members of clusters with fractional populations greater than a threshold value (usually 0.0001). The resultant basis set is clustered and the conformer populations are optimized. Each cycle of clustering-fitting-expansion is a refinement cycle with an attendant increase in the goodness-of-fit between computed and observed data. Refinement is continued until the number of structures in the active basis set is less than the number of requested clusters. If convergence is not reached, the clustering level is increased in increments of one until convergence occurs.

6. Significance Testing. The Hamiltonian version of the F-test⁴⁰ was used for testing the significance of improvements in fitting that occur as the number of variable parameters is increased. In our implementation, the number of conformers used in the fit is systematically lowered by removing the least populated conformer in the basis set, reoptimizing the populations, and comparing the ratio of the *R*-factors (eq 3) according to Hamilton's method. Typically we test for significance at a conservative

$$\omega_R = \frac{\sum_i \omega_i (|F_{i0}| - |F_{ic}|)^2}{\sum_i \omega_i |F_{i0}|^2} \quad (3)$$

(i.e. with an emphasis on removing insignificant conformers) 5% level ($\alpha = 0.05$, or a 5% probability of incorrectly retaining more structures than are justified by the data). Resulting from this procedure is a set of structures and populations that have been reduced to the minimum justifiable number of conformers.

F. Molecular Mechanics Calculations. 1. Conformational Searching of Four-Coordinate Structures. Coordinate randomization and systematic torsion angle search methods were employed in this work to search the potential energy surface of four-coordinate complexes. The first step was to randomize an initial set of either crystallographic coordinates or coordinates generated by molecular graphics by adjusting each atomic coordinate with a randomly generated multiplier. Each of the 100 structures generated was subjected to 700 steps of energy minimization using the adopted basis set Newton-Raphson algorithm (abnr). The lowest energy structure was used as a starting point for a systematic grid search; because the main degrees of conformational flexibility appeared to be rotation about the P-C_{arene} bonds, these torsions defined the potential energy grid to be searched. For each grid search, two P-C_{arene} torsion angles (ϕ and ψ) were advanced systematically in 20° increments followed by 500 steps of abnr energy minimization. Thus for the complexes containing the bisphosphines, DIPAMP and CHIRAPHOS, two ϕ - ψ maps were created, one for the set of arene angles on each phosphorus. Further fine tuning of the structure in the region of the minimum was achieved by performing another 100 coordinate randomizations as in the initial phase of the search. The lowest energy structure from this second set of randomizations was taken as the minimum. For all complexes the energy of the lowest energy conformation was observed to increase as each segment of the sequence was concluded.

2. Conformational Searching of Six-Coordinate Complexes. Parameter development for the six-coordinate dihydride rhodium complexes was patterned after the structure-based parameterization developed for the

(38) QUANTA is a registered trademark of Molecular Simulations, Inc.
(39) Solomon, I. *Phys. Rev.* 1953, 92, 953.

(40) Hamilton, W. C. *Acta Crystallogr.* 1965, 18, 502.

Table VI. Molecular Mechanics Parameters and Crystallographic and Calculated Structure Values for Rh(H)₃(TRIPHOS)

	parameter			
	r_0	k_r	r	r
Rh-P ^a	2.28	90	2.30	2.26(0.04)
Rh-H ^a	1.60	175	1.51	1.60(0.11)
P-C _{arene} ^a	1.82	214	1.84	1.82(0.03)
P-C _{alkane} ^a	1.81	232	1.84	1.84(0.00)
	ϕ_0	k_ϕ	ϕ	ϕ
P-Rh-P ^b	90.0	5.53	90	91(2)
H-Rh-H ^b	90.0	3.98	91	86(5)
P-Rh-H ^b	90.0	2.74	89	91(2)
Rh-P-C _{arene} ^c	115.0	40.0	119	117(2)
Rh-P-C _{alkane} ^c	120.0	40.0	110	113(3)
C _{arene} -P-C _{arene} ^c	98.6	50.0	100	98(2)
C _{arene} -P-C _{alkane} ^c	104.6	50.0	104	105(2)

^a Bond stretch parameters defined according to $E = k_r(r - r_0)^2$ with r in Å and k_r in kcal/mol Å. ^b Fourier bond angle parameters defined according to reference???. ^c Bond angle bending parameters defined according to $E = k_\phi(\phi - \phi_0)^2$ with ϕ in deg and k_ϕ in kcal/mol rad².

four-coordinate structures but was hampered by the lack of crystallographic structures. For the highly symmetric octahedral idealized geometry, we find that 4-fold Fourier potential energy terms for bond angles about the metal suffice: it is not necessary to use the more complex SHAPES functions with spherical internal coordinates. One crystal structure served as the model complex for the rhodium(III)-phosphorus-hydride parameter development: Rh(H)₃(TRIPHOS) (TRIPHOS = bis(1,1,1-tris(diphenylphosphinomethyl)ethane-*P,P',P''*)).⁴¹ Parameters for the Rh36, PMH, and HM atoms were optimized by adjusting initial values derived from the four-coordinate complexes to give the best match with neutron diffraction structural data. The final values are shown in Table VI.

Attempts to apply the three-step conformational space searching method that was used with four-coordinate complexes to the six-coordinate structures was unsuccessful. This failure was due to the very high potential energies incurred upon coordinate randomization. Therefore, we developed the "rubberband" protocol.

(41) Ott, J.; Venanzi, L.; Gilardi, C. A.; Midollini, S.; Orlandini, A. *J. Organomet. Chem.* **1985**, *291*, 89.

The rubberband method involves stretching the P-C_{arene} bonds, twisting them, then letting them snap back into place. The bonds were first stretched to 4 Å, and the P-C_{arene} torsion angles were systematically incremented to examine all possible combinations of ϕ and ψ values. Each of these starting structures was then brought back gently to the unstretched P-C_{arene} bond length by lowering the equilibrium bond length to its normal 1.8-Å value and slowly increasing its stretching force constant from 10% of its final value to the full final value (232 kcal/Å²). A total of 1800 minimization steps was used in bringing the stretched and twisted structure down to its final energy-minimized structure. A total of 256 stretched and twisted starting points were explored. Because the structures are so crowded, many of the other methods that we tried failed to give low-energy structures; when the barriers to conformer interconversion are high, the energies of the minimized structures are very dependent on the starting point.

Acknowledgment. Financial support from the NIH and the Monsanto Company are gratefully acknowledged. We are thankful for the helpful comments of Prof. Tony Rappè and Prof. Larry Dahl. In addition, we are grateful to referee M.T. for helpful suggestions regarding condensing of the original manuscript. The generous loan of rhodium from Johnson-Matthey is gratefully acknowledged.

Supplementary Material Available: Tables of data for the crystallographic structure determination of [Rh(DIPAMP)-(NBD)](PF₆), including Table 1, Crystal Data, Data Collection Conditions, and Solution and Refinement Details; Table 2, Atomic Coordinates and Equivalent Isotropic Displacement Parameters; Table 3, Bond Lengths; Table 4, Bond Angles; Table 5, Anisotropic Displacement Parameters; and Table 6, Hydrogen Atom Coordinates and Isotropic Displacement Parameters; tables of NOE data and ¹H NMR assignments, including Table 7, ¹H-¹H NOE Data for **1a**; Table 8, ¹H-¹H NOE Data for **2a**; and Table 9, ¹H-¹H NOE Data for **3a**; and contour plots for the ϕ - ψ searches, including Figure 1, ϕ - ψ Map for [Rh(DIPAMP)(COD)]⁺ (**1a**) with Electrostatic Interactions Included; Figure 2, ϕ - ψ Map for [Rh(DIPAMP)(NBD)]⁺ (**2a**), and Figure 3, ϕ - ψ Map for [Rh(DIPH)(MAC)]⁺ (**3c**) (28 pages). Ordering information is given on any current masthead page.